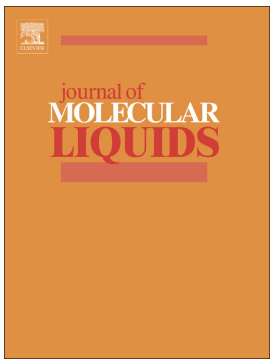

Combination of air-dispersion cathode with sacrificial iron anode generating Fe2+Fe3+2O4 nanostructures to degrade paracetamol under ultrasonic irradiation

Reza Mirzaee, Reza Darvishi Cheshmeh Soltani, Alireza Khataee, Grzegorz Boczkaj

PII: S0167-7322(19)30902-X
DOI: https://doi.org/10.1016/j.molliq.2019.04.033
Reference: MOLLIQ 10756

To appear in: *Journal of Molecular Liquids*

Received date: 15 February 2019
Revised date: 3 April 2019
Accepted date: 5 April 2019

Please cite this article as: R. Mirzaee, R.D.C. Soltani, A. Khataee, et al., Combination of air-dispersion cathode with sacrificial iron anode generating Fe2+Fe3+2O4 nanostructures to degrade paracetamol under ultrasonic irradiation, Journal of Molecular Liquids, https://doi.org/10.1016/j.molliq.2019.04.033

Combination of air-dispersion cathode with sacrificial iron anode generating $Fe^{2+}Fe^{3+}{}_2O_4$ nanostructures to degrade paracetamol under ultrasonic irradiation

Reza Mirzaee,[a] Reza Darvishi Cheshmeh Soltani,[a,*] Alireza Khataee,[b] Grzegorz Boczkaj,[c]

[a] Department of Environmental Health Engineering, School of Health, Arak University of Medical Sciences, Arak, Iran.

[b] Research Laboratory of Advanced Water and Wastewater Treatment Processes, Department of Applied Chemistry, Faculty of Chemistry, University of Tabriz, 51666-16471 Tabriz, Iran.

[c] Gdansk University of Technology, Faculty of Chemistry, Department of Process Engineering and Chemical Technology, 80 – 233 Gdansk, G. Narutowicza St. 11/12, Poland.

[*] Corresponding author:

E–mail address: darvishi@arakmu.ac.ir (rezadarvish86@yahoo.com)

Tel.: +98 86 33662024; Fax: +98 86 33686443

Abstract

In the present study, ultrasound (US) was coupled with an electrochemical process (ECP) consisting of a novel cathode of carbon cloth (CC)-carbon black (CB) as the nano-composite air-dispersion cathode (NADC) for the degradation of paracetamol (APAP) in an aquatic medium. The NADC favored in situ production of H_2O_2 by the cathodic reduction. The implementation of iron sacrificial anode instead of dimensionally stable anodes resulted in the generation of $Fe^{2+}Fe^{3+}{}_2O_4$ nanostructures in the solution. The $Fe^{2+}Fe^{3+}{}_2O_4$ nanostructures were activated by means of both US and H_2O_2 to produce more $^{\bullet}OH$ in the aqueous solution. In addition, the utilization of US caused the conversion of H_2O_2 to $^{\bullet}OH$ irrespective of free oxidizing radicals generated through cavitation phenomenon. The hybrid method based on coupling US and NADC-ECP in the presence of $Fe^{2+}Fe^{3+}{}_2O_4$ nanostructures proved synergism (39.8%) allowing to effective decomposition of APAP. The pulse mode of US enhanced the degradation efficiency of APAP as compared to the sweep and normal modes. The intermediates of the degradation route were identified using GC-MS analysis as well as mineralization efficiency. The toxicity assay was also performed based on the inhibition test using activated sludge of a biological wastewater treatment plant.

Keywords: Ultrasound; Sonocavitation; Hydrogen peroxide; Air-permeable cathode; Magnetite nanostructures; Pharmaceuticals.

1. Introduction

In recent years, the growth of public consciousness about various kinds of environmental problems has persuaded legislative organizations to limit the discharge of pollutants into terrestrial and aqueous environments. Among various environmental media, the contamination of aquatic environments by emerging pollutants such as pharmaceutically active compounds (PhACs) has attained higher interest due to their toxic effects even at low concentrations [1, 2]. In fact, a growing attention on the decontamination of PhACs-contained waters is observed. PhACs have proposed as a new classification of water pollutants, which have been detected in the aquatic environments such as rivers, lakes, reservoirs and groundwater [3]. Among PhACs, the non-steroidal anti-inflammatory pharmaceuticals such as paracetamol (APAP) are of high importance due to their large consumption for treatment purposes [3]. APAP is a widely consumed anti-inflammatory drug which is inadequately degraded in wastewater treatment systems [1, 4]. It is widely consumed for the relief of minor pains, fever, inflammation, headaches, and the treatment of cold and flu [4, 5]. PhACs such as APAP are classified as refractory organic compounds which are resistant against the conventional biological treatment technologies [6]. Therefore, research studies are conducted to initiate novel and efficient treatment methods than those currently used in environmental remediation. In this regard, advanced oxidation processes (AOPs) such as photocatalysis [1, 7], sonocatalysis [8, 9], Fenton [10, 11], and electroFenton [6] have been proposed as efficient treatment technologies for the elimination of PhACs in the aqueous phase owing to the generation of free hydroxyl radical ($^{\bullet}OH$) with very high oxidizing potential compared with conventional oxidizing agents. Hydroxyl radical, as a non-selective oxidizing agent, can effectively degrade APAP to less toxic or even non-toxic compounds within a short reaction time [10]. The electrochemical AOPs

(EAOPs) are an attractive group of treatment processes for degrading emerging pollutants such as pharmaceuticals [2, 12-14]. The direct anodic oxidation via various dimensionally stable anodes is proposed as the main category of EAOPs. During the direct anodic oxidation, $^{\bullet}OH$ is generated by the dissociation of water molecules when stable anodes are used. In our previous works, Pt anode was applied as the stable anode where an air-dispersion electrode was implemented as porous cathode for the reductive production of hydrogen peroxide as represented in Eq. (1) [2, 15-17]:

$$O_2 + 2H^+ + 2e^- \rightarrow H_2O_2 \quad (1)$$

The addition of Fe ions chemical sources to the abovementioned electrochemical process could be resulted in the generation of $^{\bullet}OH$ in the solution based on Fenton reaction. In an innovative manner, in the present study, iron anode was utilized as sacrificial anode in order to generate $Fe^{2+}Fe^{3+}{}_2O_4$ (magnetite) particles in the oxygen-free solution on the basis of the Schikorr reaction [18]:

$$3Fe(OH)_2 \rightarrow Fe_3O_4(FeO \cdot Fe_2O_3) + H_2 + 2H_2O \quad (2)$$

Consequently, $^{\bullet}OH$ can be formed as a result of the interaction between in situ generated H_2O_2 and as-generated $Fe^{2+}Fe^{3+}{}_2O_4$ particles through the Fenton reaction, which is shown in Eqs. (3) and (4) [17, 19-23]:

$$Fe^{3+} + H_2O_2 \rightarrow Fe^{2+} + HO_2^{\bullet} + H^+ \quad (3)$$

$$Fe^{2+} + H_2O_2 \rightarrow Fe^{3+} + OH^- + {}^{\bullet}OH \quad (4)$$

Nowadays, researches on the decomposition of PhACs by means of AOPs have focused on the application of sonocavitation based AOPs [5, 24-26]. Furthermore, the US has been coupled with

conventional electrochemical treatment processes in order to improve the decomposition efficiency [24, 27]. In the present study, the US was combined with an electrochemical process (ECP) equipped with air-dispersion cathode and iron sacrificial anode instead of conventional configurations. The irradiation of US can result in the activation of as-generated $Fe^{2+}Fe^{3+}{}_2O_4$ particles to generate more $^{\bullet}OH$ in the bulk solution according to the following equation [28, 29]:

$$Fe^{3+} + H_2O + US \rightarrow Fe^{2+} + {}^{\bullet}OH + H^{+} \quad (5)$$

The porous cathode was comprised of a flexible carbon cloth (CC) covered by carbon black (CB) nanoparticles in order to enhance the mechanical and electrical properties of the as-prepared nanocomposite air-dispersion cathode (NADC). In summary, the integration of US with both $Fe^{2+}Fe^{3+}{}_2O_4$ nanostructures released from sacrificial anode and H_2O_2 generated by NADC could be very effective for highly efficient production of free radical species in the bulk solution to synergistically degrade the APAP molecules. Based on our hypothesis, these three factors could serve as an effective triangle for synergistic decomposition of the refractory target pollutant. To the best of our knowledge, the treatment system described above has not been used in any study to decompose various environmental pollutants.

2. Materials and methods

2.1. Chemicals and preparations

APAP with molecular structure of $C_8H_9NO_2$ and molecular weight of 206.29 g/mol was prepared from Sigma-Aldrich (USA). The CB (VULCAN, XC72R) was obtained from Cabot Co. (USA). Teflon-treated CC (thickness: 0.11 mm) and PTFE (5 wt% Teflon emulsion) were obtained from

ElectroChem, Inc (USA). The NAPC was synthesized via the procedure represented in our previous research study [2].

2.2. Experimental set-up and analytical methods

The electrochemical cell was consisted of the iron anode, NAPC and DC power supply. The ultrasonication of the cell was accomplished using an ultrasonic bath (Elma, P30H, Germany). Sodium sulfate was used as supporting electrolyte of the ECP. For the analysis, 10-mL samples were withdrawn from the reactor. Then, they were centrifuged for 5 min at 10000 rpm. The residual concentration of APAP in as-prepared samples was determined utilizing high performance liquid chromatography (HPLC, Agilent Co.). The measuring device was equipped with a reversed-phase C18 column and an UV detector adjusted to the wavelength of 242 nm. Acetonitrile and phosphate buffer (pH = 4.8) were mixed to use as mobile phase (volumetric ratio of 15:85). The flow rate of the mobile phase was 1 mL/min. The concentration of hydrogen peroxide generated through the cathodic reduction was measured as follows: 4-mL samples were withdrawn from the bulk solution. Then 3 mL iodide reagent [potassium iodide (0.4 M), ammonium molybdate (10^{-4} M), and sodium hydroxide (0.06 M)] and 3 mL buffer solution (0.1 M potassium biphthalate) were added to each collected sample. The absorbance of the samples was measured at wavelength of 351 nm by means of a UV-Vis spectrophotometer (Hach Co, USA). The role of main operational parameters, including initial pH, APAP concentration, electrolyte concentration, current intensity, US frequency, US power, and irradiation mode was evaluated to reach a better understanding of the performance of treatment process. In the following, the treatment processes were kinetically evaluated. Preliminary evaluation of the data

revealed that a pseudo-first order kinetic model can be used for this purpose. The present study was further aimed to identify as-generated organic and inorganic byproducts during the decomposition of APAP by the combined process by means of gas chromatography-mass spectroscopy (GC-MS) technique (GC Agilent 7890 MS Agilent 5975, USA). For this purpose a HP-5 capillary column was used with helium as carrier gas (flow rate of 1 mL/min; injection mode – split 10:1).

2.3. Characterization

For the surface characterization of NADC, Field emission scanning electron microscopy was utilized (TESCAN FE-SEM, Model: Mira3, Czech Republic). The crystallinity of the samples was evaluated via X-ray diffraction (PANalytical XRD, X'Pert Pro MPD, the Netherlands). The thermal stability of the air-dispersion cathode was assessed using the thermogravimetric analysis accompanied by derivative TGA (TGA/DTG) (TA thermogravimetric analyzer, SDT Q600, USA) under Ar atmosphere. The stability of the samples was checked within the heating range of 25-600 ^{o}C based on the adjusted heating rate of 10 ^{o}C/min. The mass of sample was 2.83 mg to avoid any possible influence of the mass and heat transfer limitations.

2.4. Activated sludge inhibition test

The toxicity of the effluents after various treatment processes was assayed through activated sludge inhibitory examination. In this procedure, the return activated sludge of the biological activated sludge process with mixed liquor volatile suspended solids (MLVSS) of about 1770

mg/L was used. The MLVSS was determined according to our previous research work. Oxygen uptake rate (OUR) of the activated sludge sample was measured after the addition of various effluents (US alone, NADC-ECP alone and US/NADC-ECP effluents) using dissolved oxygen meter (WTW, Oxi 3205, Germany). According to the results, the oxygen consumption inhibition [I_{OUR}(%)] was calculated using below equation:

$$I_{OUR}\ (\%) = \left[1 - \frac{OUR_S}{OUR_B}\right] \times 100 \qquad (6)$$

where OUR_S and OUR_B were the OUR of the sample containing APAP and the OUR of the blank sample.

3. Results and discussion

3.1. Characterization

3.1.1. FE-SEM and XRD

FE-SEM analysis was accomplished to evaluate surface morphology of the particles generated during the anodic corrosion. The images were exhibited in Fig. 1 (a) and (b) with different scales. As shown, the formation of particles in nano-size (<100 nm) can be clearly seen in Fig. 1 (b). In the following, XRD analysis was performed to identify the phase and crystallinity of the nanostructures (Fig. 1 (c)). The peaks placed at 30.54 (220), 35.89 (311), 43.44 (400), 53.79 (422), 57.49 (511), 62.94 (440) and 74.39^o (533) were related to magnetite ($Fe^{2+}Fe^{3+}{}_2O_4$) structure (JCPDS card number of 19–0629) [30] with no impurity peak in the obtained pattern. Moreover, an appropriate crystalline structure was attained for the $Fe^{2+}Fe^{3+}{}_2O_4$ nanostructures. In the case of porous cathode, the FE-SEM image of pure CB indicated the nano-size of CB

particles with spherical shapes to be acted as a suitable conductive coating agent for the porous cathode (Fig. 2 (a-1)). As shown, the nanoparticles in grape-like clusters did not show obvious boundaries. The corresponding XRD pattern of pure CB was depicted in Fig. 2 (a-2). As shown, the broad peak in the pattern of CB centered at 23.41° was attributed to the (002) plane of carbonaceous materials [31]. In addition, the broad peak centered at 43.46° was also related to the (100) plane of the carbonaceous substance. The FE-SEM image of pure CC was also taken. The carbonaceous strings can be clearly seen in Fig. 2 (b-1). Moreover, some nanostructured shards on the surface of the strings were observed by means of the obtained FE-SEM image. The presence of these nanostructured shards could be beneficial for the efficient incorporation of CB nanoparticles into the CC porous structure. The corresponding XRD pattern of CC was displayed in Fig. 2 (b-2). The intense peak located at 18.16° and the weak peak placed at 36.76° confirmed the presence of Teflon in the structure of PTFE-treated CC [32]. The peak placed at 25.21° was associated with the carbonaceous structure of CC. Fig. 2 (c-1) showed the appropriate immobilization of CB nanoparticles on the surface of CC strings. The favorable coverage of the surface of the CC by CB nanoparticles is quite evident. The CB nanoparticles were aggregated on the surface of CC to some extent. However, this aggregation resulted in the creation of numerous pores in grape-like clusters. Evaluation of the crystalline structure of CB-coated CC showed no significant change in the pattern of CC after being covered with CB nanoparticles (Fig. 2 (c-2)). In fact, the composition of the CB nanoparticles would not significantly modify the CC structure.

3.1.2. TGA/DTG

The stability of the samples at different temperatures was checked via TGA/DTG analysis. Fig. 3 exhibits the TGA/DTG graphs of both uncoated and CB-coated CC. In the case of uncoated CC, the total weight loss of 23.91% was obtained in the temperature range of 25–600 ^{o}C (Fig. 3 (a)). The peak in the DTG curve indicated the temperature at which the maximum drop in weight occurred. As can be clearly seen, the maximum drop in the weight of uncoated CC was observed at about 570 ^{o}C, which was due to the thermal degradation. It can be also concluded that the material is thermally stable (no weight loss) up to approx. 500 ^{o}C. In the case of CB-coated CC, two main peaks were observed in the DTG curve (Fig. 3 (b)). The first was observed at 501 ^{o}C and the latter at 557 ^{o}C. This was attributed to the presence of CB nanostructures in the interconnected structure of CC. The weight drop of CB-coated CC was obtained to be 50% within the temperature range of 25-600 ^{o}C. Actually, CB has a polyaromatic structure which is produced through the partial combustion of gaseous or liquid hydrocarbons. Hence, the significant weight loss of CB-coated CC could be ascribed to the thermal cracking of the polyaromatics in the structure of CB, which initiated the thermal degradation of the CB-coated CC [33].

3.2. Comparison

Fig. 4 exhibited the removal of APAP by using US alone, NADC-ECP alone, and US coupled with NADC-ECP. Although the application of US inducing sonocavitation is proposed as the efficient method of organic compound degradation [34, 35], the application of control process of US alone resulted in only a small degradation of APAP (13.8%) within 90 min. Consequently, the efficiency of sole use of US for degrading APAP was low. As shown in Fig. 4, the reaction

rate constant obtained for the US alone was 1.7×10^{-3} min^{-1} based on the pseudo-first order kinetic model with high correlation coefficient of 0.95. The energy of ultrasounds induces formation and growth of "cavitation bubbles" in water samples related to the sonocavitation phenomenon. The micro-bubbles will reach the resonance size that is the average size of the micro-bubble before undergoing the violent collapse [20]. The collapse of the micro-bubbles makes extreme temperature and pressure in the bulk solution. These conditions generate free hydroxyl radical ($^{\bullet}OH$) which further react with the target compound [4, 8, 36-38]:

$$H_2O + US \rightarrow H^{\bullet} + {}^{\bullet}OH \quad (7)$$

The results of the present study indicated the generation of an insignificant quantity of $^{\bullet}OH$ during the US treatment process. In accordance with our results, it is demonstrated that the efficiency of US as a sole process of treatment for the degradation of the target pollutants in many cases is insignificant and time-consuming [39, 40]. Thus, this treatment process is coupled with other treatment processes to efficiently degrade the target pollutant in a short period of reaction time. At the same operational conditions, the NADC-equipped ECP showed the APAP removal efficiency of 32.6% in the presence of electro-generated $Fe^{2+}Fe^{3+}{}_2O_4$ nanostructures. The reaction rate constant obtained for the ECP alone was 4.2×10^{-3} min^{-1} with high correlation coefficient of 0.96. In the NADC-equipped ECP operated for the electro-reduction of O_2 gas to generate H_2O_2, as-generated H_2O_2 can directly degrade APAP molecules to some extent. Interestingly, H_2O_2 can interact with electro-generated $Fe^{2+}Fe^{3+}{}_2O_4$ nanostructures to generate $HO^{\bullet}$ during the ECP as shown in Eqs. (3) and (4). Moreover, electro-generated H_2O_2 can react with $H^{\bullet}$ (see in Eq. 6) to produce more $^{\bullet}OH$ in the liquid phase as exhibited in the following equation [20, 41]:

$$H_2O_2 + H^{\bullet} \rightarrow H_2O + {}^{\bullet}OH \quad (8)$$

Previous studies proved synergistic effect of combining H_2O_2 with cavitation-based processes, which results in efficient conversion of H_2O_2 molecules to $H^{\bullet}$ even in strongly basic pH conditions, where normally H_2O_2 decompose to less reactive radical species [42-44]. The integration of US with NADC-ECP led to the promising solution for further enhancement of APAP degradation. The degradation efficiency of 60.8% was obtained after 90 min by using the integrated process with the APAP decomposition rate of 9.8×10^{-3} min^{-1}. Thus, the assistance of US irradiation could significantly increase the degradation of APAP in the presence of $Fe^{2+}Fe^{3+}{}_2O_4$ nanostructures. Lan et al. observed a 50% increase in the degradation efficiency of naproxen when US was coupled with the Fenton process [45]. The following equation was implemented to calculate the synergy percent (%) of the integrated process in term of APAP degradation [8, 46]:

$$Synergy\ (\%) = 1 - \frac{k_{US}+k_{NADC-ECP}}{k_{US/NADC-ECP}} \times 100 \quad (9)$$

where k_{US}, $k_{NADC\text{-}ECP}$ and $k_{US/NADC\text{-}ECP}$ are reaction rate constants of US alone, ECP alone and the integrated process of US/NADC-ECP, respectively. Accordingly, the synergy for the integrated process was almost 40%. This synergy could be attributed to the increased conversion rate of H_2O_2 molecules, produced via cathodic reduction, to $^{\bullet}OH$ as a result of US irradiation which is represented below:

$$H_2O_2 + US \rightarrow {}^{\bullet}OH + {}^{\bullet}OH \quad (10)$$

The $Fe^{2+}Fe^{3+}{}_2O_4$ nanostructures produced via anodic corrosion could generate $^{\bullet}OH$ when the solution was ultrasonically irradiated (see Eq. 5). Moreover, the passive film generated on the

surface of the iron sacrificial anode would be removed due to the US waves and collapse of the cavitation bubbles, resulting in decreasing the mass transfer resistance and increasing the generation of $Fe^{2+}Fe^{3+}{}_2O_4$ nanostructures [47]. To verify the generation of free radical in the bulk solution and its role in the decomposition of APAP molecules, the decomposition efficiency of the treatment process was compared in the presence and absence of ethyl alcohol (0.05 M). The substantial reduction in the decomposition efficiency (%) of APAP from 60.8 to 49.2% was observed when the radical scavenging compound (ethyl alcohol) was added to the solution, indirectly verifying the generation of free oxidizing radicals in the solution and their significant role in the decomposition of APAP molecules.

3.2.1. Contribution of adsorption

To specify the role of adsorption in the elimination of the target pollutant, the EC process equipped with NAPC and iron anode was operated in the absence of APAP. For this purpose, the electrodes were withdrawn from the EC cell at the end of the reaction and then specific amount of APAP (5 mg/L) was added to the solution containing electro-generated $Fe^{2+}Fe^{3+}{}_2O_4$ nanostructures. Afterwards, the solution was magnetically stirred for 90 min to achieve the adsorption of APAP onto $Fe^{2+}Fe^{3+}{}_2O_4$ nanostructures. In the following, the adsorption data were modeled using the linearized forms of Langmuir and Freundlich isotherm models as shown in the following equations [48-52]:

Freundlich model: $$logq_e = logK_f + \frac{1}{n} logC_e \quad (11)$$

Langmuir model: $$\frac{C_e}{q_e} = \frac{1}{kq_m} + \frac{1}{q_m} C_e \quad (12)$$

According to the results (Table 1), the adsorption of APAP by electro-generated $Fe^{2+}Fe^{3+}{}_2O_4$ nanostructures followed the Langmuir model (R^2=0.99). On the basis of Langmuir model, the maximum adsorption capacity (q_m) of $Fe^{2+}Fe^{3+}{}_2O_4$ nanostructures for adsorbing APAP was obtained to be 2.76 (mg/g), indicating the insignificant role of the adsorption process in removing APAP molecules during the integrated treatment process of US/NADC-ECP.

3.3. Operational conditions

3.3.1. Initial pH

The effect of the initial pH on the reactor performance was evaluated under four distinct pH values (pH: 3 (acidic), pH: 5.5 (natural), pH: 7 (neutral), and pH: 9 (basic)). Fig. 5 (a) showed that increasing the initial pH from 3 to 9 led to diminishing the removal efficiency of APAP from 66 to 44.8%. Overall, the acidic condition favored the degradation of APAP by means of US/NADC-ECP in the presence of electro-generated $Fe^{2+}Fe^{3+}{}_2O_4$ nanostructures. The influence of the solution pH on the degradation of APAP could be attributed to the change in its chemical structure as a function of pH fluctuations. The hydrophobic structure of APAP molecules inhibited them to be entered inside the cavitation bubbles. Therefore, they could be destroyed by $^{\bullet}OH$ radicals in the bulk solution and/or at the surface of cavitation bubbles. The pK_a value of APAP is about 9.5. Thus, APAP molecules are in non-ionic form in the acidic solution. This resulted in increasing the hydrophobicity of APAP molecules and their accumulation onto the interface of the as-generated cavitation bubbles, where higher amounts of $^{\bullet}OH$ were present [4]. Furthermore, it is well known that the increase of the solution pH lowers the oxidation potential of $^{\bullet}OH$ [19].

3.3.2. Current and H_2O_2 evolution

Fig. 5 (b) displayed that the degradation of APAP increased proportionally with current intensity. The degradation efficiency increased from 42.0 to 71.8% when the current increased from 0.05 to 0.15 A. It follows from the higher effectiveness of $^{\bullet}OH$ generation at increased current intensity of the NADC-ECP. Moreover, the increase of the current accelerates the rate of mass transfer in the solution, resulting in the increased decomposition of the target pollutant [2]. In addition, the corrosion of iron sacrificial anode providing formation of $Fe^{2+}Fe^{3+}{}_2O_4$ nanostructures could be also improved in terms of the increased mass transfer rate [47]. As depicted in Fig. 5 (b), the generation of H_2O_2 in the solution through the cathodic reduction was proportional to the applied current intensity. Overall, the increased current results in the higher oxygen reduction rate, generating more H_2O_2 molecules in the solution [53]. At currents of 0.05, 0.1, and 0.15 A, the concentration of electro-generated H_2O_2 was 107.7, 137.4, and 151.3 μM, respectively. The low generation of H_2O_2 via NADC could be associated with its self-decomposition in an undivided cell for operating ECP [15]:

$$H_2O_2 \rightarrow HO_2^{\bullet} + H^+ + e^- \qquad (13)$$

This fact should be taken into consideration that the optimum amount of electro-generated H_2O_2 is favorable for the generation of $^{\bullet}OH$ in the bulk solution. As-generated H_2O_2 can be a radical scavenger at excessive concentrations. In addition, as-generated H_2O_2 is practically not accumulated in the NADC-ECP process owing to the significant amounts of magnetite nanoparticles produced via the sacrificial anode. At the end of the NADC-ECP process, about 27

mg magnetite nanoparticles were released into the solution within 90 min due to the anodic corrosion.

3.3.3. Solute and Na_2SO_4 concentration

The drug concentration in pharmaceutical industries wastewater often varies to some extent. Thus, the effectiveness of the treatment process under different pollutant concentrations must be assessed. For this purpose, the initial concentration of APAP was varied between 3 and 10 mg/L. The degradation efficiency (%) of APAP was found to be 83% at the APAP concentration of 3 mg/L (Fig. 5 (c)). As a result, the degradation efficiency was minimal (12.2%) at APAP concentration of 10 mg/L. Clearly, the more APAP molecules in the reactor, the higher amounts of oxidizing agents are required for the effective decomposition [54]. In the next step, the effect of electrolyte concentration on the degradation efficiency of APAP was assessed by varying the initial sodium sulfate concentration between 0.02 and 0.07 M. Increasing the electrolyte concentration in the abovementioned range resulted in increasing the degradation efficiency of APAP from 43.8 to 68.4% (Fig. 5 (d)). Using higher concentrations of Na_2SO_4 was desirable for the solution conductivity and the transfer rate of the reactants, which led to the intensified decomposition of APAP. Under US irradiation, increasing the amount of Na_2SO_4 as the electrolyte of NADC-ECP favored the generation of $SO_4^{\bullet-}$ and subsequently, $^{\bullet}OH$ as represented in the following equations [2, 55]:

$$SO_4^{2-} + {}^{\bullet}OH \rightarrow SO_4^{\bullet-} + OH^- \quad (14)$$

$$SO_4^{\bullet-} + H_2O \xrightarrow{US} SO_4^{2-} + {}^{\bullet}OH + H^+ \quad (15)$$

Additionally, higher concentrations of the supporting electrolyte could be beneficial to enhance the electro-generation of H_2O_2 [56].

3.3.4. US effect (Irradiation mode, frequency and power)

The cavitation phenomenon, especially the size of cavitation bubbles, depends on the US characteristics (frequency/power) and sono-reactor type [57]. Hence, the effect of irradiation mode of US (normal, sweep, and pulse) as well as the effect of US power and US frequency was studied. The results were illustrated in Fig. 6. For each irradiation mode, the enhanced degradation of APAP was obtained when the applied power increased from 50 to 100%. Increasing the power intensity, defined as the input power to the transmitting area ratio, results in the intensified acoustic pressure, higher amounts of cavitation phenomenon, and subsequently, more collapse of cavitation bubbles for the generation of $^{\bullet}OH$ in the solution. The relationship between the acoustic pressure and US power intensity can be represented as the following equation [25]:

$$I = \frac{P_0^2}{2\rho C} \quad (16)$$

where I, P_0, ρ, and C are the US power intensity (W), the acoustic pressure (Pa), the solution density (kg/m^3), and the sound speed in the solution (m/s), respectively. Contrary to the results of our previous study where US/catalyst was used for degradation of organic azo dye, the results of the present study revealed that high frequency of US (80 kHz) was more effective than the low frequency (37 kHz). It has been reported that the best results in terms of sonocavitational degradation of organic compounds were obtained for high frequencies [35]. The US frequency is

defined as the number of repeating events taking place per unit of time. Increasing the frequency decreases the lifetime of the as-generated cavitation bubbles. This leads to the increased power of the bubbles collapse as well as the number of collapse events per unit of time, resulting in increased generation of $^{\bullet}OH$ and stronger micro-fluctuations in the fluid enhancing the transport of chemical species across the interface. From another viewpoint, a shorter lifetime owing to the high frequency favors the ejection of $^{\bullet}OH$ into the bulk before their recombination [25]. Similar results have been reported by other researchers during the application of US-assisted degradation of various pharmaceutical compounds [58-60]. However, increasing the frequency caused slight increase in the degradation of APAP, which may be due to the formation of less energetic cavitation bubbles with weak collapse irrespective of higher $^{\bullet}OH$ formation at higher US frequencies [24]. At normal mode of irradiation with frequency of 37 kHz, increasing the power from 50 to 100% resulted in increasing the degradation efficiency from 50.3 to 60.8%, respectively, while the increase in the degradation efficiency was from 51.5 to 77.1% at US frequency of 80 kHz. According to the results, the implementation of pulse mode of US irradiation considerably increased the degradation of APAP compared with the sweep and normal modes. At frequency of 80 kHz with 100% US power, the degradation efficiencies were found to be 77.1, 71.6 and 86.6% when normal, sweep and pulse modes of irradiation were implemented, respectively. It is reported that the implementation of US in pulse mode can be resulted in the intensified degradation of organic compounds [61-63]. Therefore, the application of pulse mode of US can be persuasive considering the fact that the operation of US in repeating cycles also reduces the power consumption. The implementation of pulse mode leads to the accumulation of APAP molecules on the surface of cavitation bubbles during the off-times, thereby enhancing the decomposition of more APAP molecules due to the cavitation

phenomenon. On the other hand, improving the diffusion rate of the hydrophobic pollutants into the vicinity of the cavitation bubbles during the Off-times leads to the improved chemical decomposition of the target pollutant. In addition, the application of pulsed US with repeated cycles diminishes the shielding effect due to reducing wave scattering, thereby increasing the efficiency of the US-based treatment technique. In general, the pulse mode of US is more chemically reactive than the normal mode at the same frequency and power input. Further, the pulsed US brings about the spatial expansion of active zones in the bulk solution for the destruction of pollutant [61].

3.4. Intermediates determination

According to the results of GC-MS analysis, some relevant intermediates produced during the degradation of APAP by means of US/NADC-ECP were identified. In accordance with the obtained intermediates, two main pathways for the degradation of APAP were proposed and illustrated in Fig. 7. As represented, the generation of intermediate byproducts with lower molecular weights during the decay of APAP confirmed the effectiveness of the applied treatment process. The APAP can be initially oxidized via $^{\bullet}OH$ attack to the aromatic ring at ortho, meta, and para positions considering hydroxyl groups of the compound (hydroxylation) [7]. As a result, the as-generated $^{\bullet}OH$ favored to attack the para position of APAP regarding hydroxyl functional groups. This attack produced the hydroquinone intermediate as represented in the proposed reaction pathways [64]. Interestingly, as-generated hydroquinone intermediate can enhance the decomposition of the target pollutant degradation. Actually, the high reducing potential of hydroquinone leads to the regeneration of Fe^{2+} from Fe^{3+} ions in the structure of

magnetite nanostructures, improving the formation of $^{\bullet}OH$ according to Eqs. (3) and (4). The reduction of hydroquinone resulted in the formation of benzoquinone as represented in the following equations [10]:

$$C_6H_6O_2 + Fe^{3+} \rightarrow C_6H_5O_2^{\bullet} + Fe^{2+} + H^+ \quad (17)$$

$$C_6H_5O_2^{\bullet} + Fe^{3+} \rightarrow C_6H_4O_2 + Fe^{2+} + H^+ \quad (18)$$

Thus, the formation of some intermediates during the treatment process may lead to the enhanced degradation of the parent compound and its organic intermediates. The formation of ortho and para benzoquinones has been reported by Villota et al., in their study on photo-Fenton degradation of APAP [65]. However, the benzoquinones generated through the successive oxidation of hydroquinone by $^{\bullet}OH$ are fairly unstable and have a tendency to undertake ring cleavage followed by further degradation. The proposed pathways also demonstrated the appropriate progress in mineralizing the parent organic compound. For this, the progress in the mineralization of APAP by the hybrid process was checked through both chemical oxygen demand (COD) and total organic carbon (TOC) analyses (Experimental conditions: $[APAP]_0$: 5 mg/L, current: 0.1 A, initial pH: natural (5.5), and electrolyte concentration: 0.04 M). Accordingly, the COD and TOC removal efficiencies of 43.5 and 30.6% were obtained at aforementioned operational conditions, respectively. The results indicated the progress in the mineralization of the target pollutant; however, more reaction time is needed to achieve the complete mineralization. The acceptable mineralization of the organic pollutant is desirable before the discharge of the reactor effluent into the ecosystem in order to avoid the health and environmental problems of the toxic refractory organics.

3.5. Bio-toxicity assay results

Despite the decomposition of the target organic contaminant, the intermediate byproducts of the contaminant generated during the catalytic destruction can cause toxicity to living organisms. Hence, the effluents of various processes involved in the decomposition of APAP including the US alone, NADC-ECP alone, and the hybrid process of US/NADC-ECP were collected for the toxicity assay on the basis of the inhibition test using activated sludge. The results showed that the values of I_{OUR} (%) decreased from 47.1 to 36.9, 31.8, and 16.5% when the effluents of the US alone, NADC-ECP alone, and US/NADC-ECP processes were fed into the return activated sludge sample (Fig. 8). Therefore, the treatment processes involved in the decomposition of APAP could convert it to less toxic byproducts. The effluent of US/NADC-ECP process caused the lowest inhibiting effect on the respiration rate of living organism in the activated sludge. In the case of the US/NADC-ECP process, the slight increase in I_{OUR} (decrease in OUR) might be ascribed to the formation of toxic substances at first stages of the degradation process. As shown in Fig. 8, increasing the elapsed time resulted in the production of effluent with lower toxicity for living organisms. This achievement verified that the effluent of the US/NADC-ECP process can be further treated by a subsequent biological treatment process without significant effect on biological treatment system. In fact, the application of US/NADC-ECP process led to increasing the biodegradability potential of the APAP-containing solution in comparison with the US and NADC-ECP alone.

4. Conclusions

Iron sacrificial anode was applied for electrochemical generation of $Fe^{2+}Fe^{3+}{}_2O_4$ nanostructures in an ECP equipped with NADC. As-generated $Fe^{2+}Fe^{3+}{}_2O_4$ nanostructures could be activated with electro-synthesized H_2O_2 for the production of $^{\bullet}OH$. Further, NADC-ECP was coupled with US in order to intensify the production of $^{\bullet}OH$ in the bulk solution through the conversion of in situ generated hydrogen peroxide as well as the activation of $Fe^{2+}Fe^{3+}{}_2O_4$ nanostructures. Neither US alone (13.8%) nor NADC-ECP alone (32.6%) could efficiently degrade APAP in the solution, while the application of US/NADC-ECP (60.8%) synergistically enhanced the degradation of APAP in comparison with the individual processes. Increasing Na_2SO_4 concentration, along with the current, increased the degradation of APAP, while increasing the initial solute concentration suppressed its removal efficiency. According to the results, the treatment process of US/NADC-ECP was pH dependent. Increasing both power intensity and frequency of US irradiation enhanced the efficiency. The best results were obtained when the pulse mode of US was operated. The identified intermediate byproducts showed the acceptable progress in the mineralization of the target refractory organic compounds during the integrated treatment process. According to the inhibitory test results, the US/NADC-ECP process produced the effluent with the lowest inhibition impact on the living organisms of the activated sludge sample.

Acknowledgements

This research project was financially supported by the National Institutes for Medical Research Development (NIMAD), Tehran, Iran (award no. 971373). Instrumental support of the Arak University of Medical Sciences (Iran) is also appreciated.

References

[1] A. Ziylan-Yavaş, N.H. Ince, Enhanced photo-degradation of paracetamol on n-platinum-loaded TiO_2: The effect of ultrasound and OH/hole scavengers, Chemosphere, 162 (2016) 324-332.

[2] R. Darvishi Cheshmeh Soltani, M. Mashayekhi, Decomposition of ibuprofen in water via an electrochemical process with nano-sized carbon black-coated carbon cloth as oxygen-permeable cathode integrated with ultrasound, Chemosphere, 194 (2018) 471-480.

[3] Y. He, Y. Dong, W. Huang, X. Tang, H. Liu, H. Lin, H. Li, Investigation of boron-doped diamond on porous Ti for electrochemical oxidation of acetaminophen pharmaceutical drug, Journal of Electroanalytical Chemistry, 759 (2015) 167-173.

[4] E. Villaroel, J. Silva-Agredo, C. Petrier, G. Taborda, R.A. Torres-Palma, Ultrasonic degradation of acetaminophen in water: Effect of sonochemical parameters and water matrix, Ultrasonics sonochemistry, 21 (2014) 1763-1769.

[5] J.-K. Im, J. Yoon, N. Her, J. Han, K.-D. Zoh, Y. Yoon, Sonocatalytic-TiO_2 nanotube, Fenton, and CCl_4 reactions for enhanced oxidation, and their applications to acetaminophen and naproxen degradation, Separation and Purification Technology, 141 (2015) 1-9.

[6] C.-C. Su, C.A. Cada, M.L.P. Dalida, M.-C. Lu, Effect of UV light on acetaminophen degradation in the electro-Fenton process, Separation and Purification Technology, 120 (2013) 43-51.

[7] L. Yang, L.E. Yu, M.B. Ray, Photocatalytic Oxidation of Paracetamol: Dominant Reactants, Intermediates, and Reaction Mechanisms, Environmental Science & Technology, 43 (2009) 460-465.

[8] R. Darvishi Cheshmeh Soltani, M. Mashayekhi, A. Khataee, M.J. Ghanadzadeh, M. Sillanpää, Hybrid sonocatalysis/electrolysis process for intensified decomposition of amoxicillin in aqueous solution in the presence of magnesium oxide nanocatalyst, Journal of Industrial and Engineering Chemistry, 64 (2018) 373-382.

[9] R.D.C. Soltani, M. Mashayekhi, M. Naderi, G. Boczkaj, S. Jorfi, M. Safari, Sonocatalytic degradation of tetracycline antibiotic using zinc oxide nanostructures loaded on nano-cellulose from waste straw as nanosonocatalyst, Ultrasonics Sonochemistry, 55 (2019) 117-124.

[10] M.D.G. de Luna, R.M. Briones, C.-C. Su, M.-C. Lu, Kinetics of acetaminophen degradation by Fenton oxidation in a fluidized-bed reactor, Chemosphere, 90 (2013) 1444-1448.

[11] M.D.G. de Luna, M.L. Veciana, J.I. Colades, C.-C. Su, M.-C. Lu, Factors that influence degradation of acetaminophen by Fenton processes, Journal of the Taiwan Institute of Chemical Engineers, 45 (2014) 565-570.

[12] O. García-Rodríguez, J.A. Bañuelos, A. El-Ghenymy, L.A. Godínez, E. Brillas, F.J. Rodríguez-Valadez, Use of a carbon felt–iron oxide air-diffusion cathode for the mineralization of Malachite Green dye by heterogeneous electro-Fenton and UVA photoelectro-Fenton processes, Journal of Electroanalytical Chemistry, 767 (2016) 40-48.

[13] V.K. Sandhwar, B. Prasad, Comparative study of electrochemical oxidation and electrochemical Fenton processes for simultaneous degradation of phthalic and para-toluic acids from aqueous medium, Journal of Molecular Liquids, 243 (2017) 519-532.

[14] S. Ahmadzadeh, M. Dolatabadi, Modeling and kinetics study of electrochemical peroxidation process for mineralization of bisphenol A; a new paradigm for groundwater treatment, Journal of Molecular Liquids, 254 (2018) 76-82.

[15] R.D.C. Soltani, A. Rezaee, A.R. Khataee, H. Godini, Electrochemical generation of hydrogen peroxide using carbon black-, carbon nanotube-, and carbon black/carbon nanotube-coated gas-diffusion cathodes: Effect of operational parameters and decolorization study, Research on Chemical Intermediates, 39 (2013) 4277-4286.

[16] N. Barhoumi, L. Labiadh, M.A. Oturan, N. Oturan, A. Gadri, S. Ammar, E. Brillas, Electrochemical mineralization of the antibiotic levofloxacin by electro-Fenton-pyrite process, Chemosphere, 141 (2015) 250-257.

[17] B. Ramírez-Pereda, A. Álvarez-Gallegos, J.G. Rangel-Peraza, Y.A. Bustos-Terrones, Kinetics of Acid Orange 7 oxidation by using carbon fiber and reticulated vitreous carbon in an electro-Fenton process, Journal of Environmental Management, 213 (2018) 279-287.

[18] K. Daub, X. Zhang, L. Wang, Z. Qin, J.J. Noël, J.C. Wren, Oxide growth and conversion on carbon steel as a function of temperature over 25 and 80°C under ambient pressure, Electrochimica Acta, 56 (2011) 6661-6672.

[19] O. Acisli, A. Khataee, R. Darvishi Cheshmeh Soltani, S. Karaca, Ultrasound-assisted Fenton process using siderite nanoparticles prepared via planetary ball milling for removal of reactive yellow 81 in aqueous phase, Ultrasonics Sonochemistry, 35 (2017) 210-218.

[20] P. Sathishkumar, R.V. Mangalaraja, S. Anandan, Review on the recent improvements in sonochemical and combined sonochemical oxidation processes–A powerful tool for destruction of environmental contaminants, Renewable and Sustainable Energy Reviews, 55 (2016) 426-454.

[21] F. Gozzi, I. Sirés, S.C. de Oliveira, A. Machulek, E. Brillas, Influence of chelation on the Fenton-based electrochemical degradation of herbicide tebuthiuron, Chemosphere, 199 (2018) 709-717.

[22] E. Brillas, M.Á. Baños, M. Skoumal, P.L. Cabot, J.A. Garrido, R.M. Rodríguez, Degradation of the herbicide 2,4-DP by anodic oxidation, electro-Fenton and photoelectro-Fenton using platinum and boron-doped diamond anodes, Chemosphere, 68 (2007) 199-209.

[23] N. Flores, F. Sharif, N. Yasri, E. Brillas, I. Sirés, E.P.L. Roberts, Removal of tyrosol from water by adsorption on carbonaceous materials and electrochemical advanced oxidation processes, Chemosphere, 201 (2018) 807-815.

[24] M. Shestakova, M. Vinatoru, T.J. Mason, M. Sillanpää, Sonoelectrocatalytic decomposition of methylene blue using Ti/Ta_2O_5–SnO_2 electrodes, Ultrasonics Sonochemistry, 23 (2015) 135-141.

[25] N. Tran, P. Drogui, S. Brar, Sonochemical techniques to degrade pharmaceutical organic pollutants, Environmental chemistry letters, 13 (2015) 251-268.

[26] Z. Eren, Ultrasound as a basic and auxiliary process for dye remediation: A review, Journal of Environmental Management, 104 (2012) 127-141.

[27] M.D. Esclapez, V. Sáez, D. Milán-Yáñez, I. Tudela, O. Louisnard, J. González-García, Sonoelectrochemical treatment of water polluted with trichloroacetic acid: From sonovoltammetry to pre-pilot plant scale, Ultrasonics Sonochemistry, 17 (2010) 1010-1020.

[28] M.T. Taghizadeh, P. Seifi-Aghjekohal, Sonocatalytic degradation of 2-hydroxyethyl cellulose in the presence of some nanoparticles, Ultrasonics sonochemistry, 26 (2015) 265-272.

[29] R.D.C. Soltani, M. Mashayekhi, S. Jorfi, A. Khataee, M.-J. Ghanadzadeh, M. Sillanpää, Implementation of martite nanoparticles prepared through planetary ball milling as a heterogeneous activator of oxone for degradation of tetracycline antibiotic: Ultrasound and peroxy-enhancement, Chemosphere, 210 (2018) 699-708.

[30] M.K. Poddar, M. Arjmand, U. Sundararaj, V.S. Moholkar, Ultrasound-assisted synthesis and characterization of magnetite nanoparticles and poly(methyl methacrylate)/magnetite nanocomposites, Ultrasonics sonochemistry, 43 (2018) 38-51.

[31] J. Xia, G. He, L. Zhang, X. Sun, X. Wang, Hydrogenation of nitrophenols catalyzed by carbon black-supported nickel nanoparticles under mild conditions, Applied Catalysis B: Environmental, 180 (2016) 408-415.

[32] R.A.P.O. d'Amorim, M.I. Teixeira, L.V.E. Caldas, S.O. Souza, Physical, morphological and dosimetric characterization of the Teflon agglutinator to thermoluminescent dosimetry, Journal of Luminescence, 136 (2013) 186-190.

[33] E. Jakab, M. Omastová, Thermal decomposition of polyolefin/carbon black composites, Journal of Analytical and Applied Pyrolysis, 74 (2005) 204-214.

[34] G. Boczkaj, A. Fernandes, Wastewater treatment by means of advanced oxidation processes at basic pH conditions: A review, Chemical Engineering Journal, 320 (2017) 608-633.

[35] M. Gągol, A. Przyjazny, G. Boczkaj, Wastewater treatment by means of advanced oxidation processes based on cavitation – A review, Chemical Engineering Journal, 338 (2018) 599-627.

[36] A. Khataee, R.D.C. Soltani, A. Karimi, S.W. Joo, Sonocatalytic degradation of a textile dye over Gd-doped ZnO nanoparticles synthesized through sonochemical process, Ultrasonics Sonochemistry, 23 (2015) 219-230.

[37] A. Khataee, A. Karimi, S. Arefi-Oskoui, R. Darvishi Cheshmeh Soltani, Y. Hanifehpour, B. Soltani, S.W. Joo, Sonochemical synthesis of Pr-doped ZnO nanoparticles for sonocatalytic degradation of Acid Red 17, Ultrasonics Sonochemistry, 22 (2015) 371-381.

[38] M. Shestakova, M. Vinatoru, T.J. Mason, E. Iakovleva, M. Sillanpää, Sonoelectrochemical degradation of formic acid using Ti/Ta2O5-SnO2 electrodes, Journal of Molecular Liquids, 223 (2016) 388-394.

[39] A. Hassani, R. Darvishi Cheshmeh Soltani, M. Kıranşan, S. Karaca, C. Karaca, A. Khataee, Ultrasound-assisted adsorption of textile dyes using modified nanoclay: Central composite design optimization, Korean Journal of Chemical Engineering, 33 (2016) 178-188.

[40] C.-H. Weng, K.-L. Tsai, Ultrasound and heat enhanced persulfate oxidation activated with Fe0 aggregate for the decolorization of C.I. Direct Red 23, Ultrasonics Sonochemistry, 29 (2016) 11-18.

[41] S. Sajjadi, A. Khataee, R. Darvishi Cheshmeh Soltani, A. Hasanzadeh, N, S co-doped graphene quantum dot–decorated Fe3O4 nanostructures: Preparation, characterization and catalytic activity, Journal of Physics and Chemistry of Solids, 127 (2019) 140-150.

[42] G. Boczkaj, M. Gągol, M. Klein, A. Przyjazny, Effective method of treatment of effluents from production of bitumens under basic pH conditions using hydrodynamic cavitation aided by external oxidants, Ultrasonics Sonochemistry, 40 (2018) 969-979.

[43] M. Gągol, A. Przyjazny, G. Boczkaj, Highly effective degradation of selected groups of organic compounds by cavitation based AOPs under basic pH conditions, Ultrasonics Sonochemistry, 45 (2018) 257-266.

[44] M. Gągol, A. Przyjazny, G. Boczkaj, Effective method of treatment of industrial effluents under basic pH conditions using acoustic cavitation–A comprehensive comparison with hydrodynamic cavitation processes, Chemical Engineering and Processing-Process Intensification, 128 (2018) 103-113.

[45] R.-J. Lan, J.-T. Li, H.-W. Sun, W.-B. Su, Degradation of naproxen by combination of Fenton reagent and ultrasound irradiation: optimization using response surface methodology, Water Science and Technology, 66 (2012) 2695-2701.

[46] F. Sepyani, R. Darvishi Cheshmeh Soltani, S. Jorfi, H. Godini, M. Safari, Implementation of continuously electro-generated Fe_3O_4 nanoparticles for activation of persulfate to decompose amoxicillin antibiotic in aquatic media: UV254 and ultrasound intensification, Journal of Environmental Management, 224 (2018) 315-326.

[47] C.-C. He, C.-Y. Hu, S.-L. Lo, Evaluation of sono-electrocoagulation for the removal of Reactive Blue 19 passive film removed by ultrasound, Separation and Purification Technology, 165 (2016) 107-113.

[48] R.D.C. Soltani, A. Rezaee, G.S. Khorramabadi, K. Yaghmaeian, Optimization of lead (II) biosorption in an aqueous solution using chemically modified aerobic digested sludge, Water Science and Technology, 63 (2011) 129-135.

[49] A. Hassani, M. Kiranşan, R. Darvishi Cheshmeh Soltani, A. Khataee, S. Karaca, Optimization of the adsorption of a textile dye onto nanoclay using a central composite design, Turkish Journal of Chemistry, 39 (2015) 734-749.

[50] H. Li, H. Lei, Q. Yu, Z. Li, X. Feng, B. Yang, Effect of low frequency ultrasonic irradiation on the sonoelectro-Fenton degradation of cationic red X-GRL, Chemical Engineering Journal, 160 (2010) 417-422.

[51] R.D.C. Soltani, A.J. Jafari, G.S. Khorramabadi, Investigation of cadmium (II) ions biosorption onto pretreated dried activated sludge, American Journal of Environmental Sciences, 5 (2009) 41-46.

[52] M. Safari, A. Khataee, R. Darvishi Cheshmeh Soltani, R. Rezaee, Ultrasonically facilitated adsorption of an azo dye onto nanostructures obtained from cellulosic wastes of broom and cooler straw, Journal of Colloid and Interface Science, 522 (2018) 228-241.

[53] X. Yu, M. Zhou, G. Ren, L. Ma, A novel dual gas diffusion electrodes system for efficient hydrogen peroxide generation used in electro-Fenton, Chemical Engineering Journal, 263 (2015) 92-100.

[54] S. Sajjadi, A. Khataee, R. Darvishi Cheshmeh Soltani, N. Bagheri, A. Karimi, A. Ebadi Fard Azar, Implementation of magnetic Fe_3O_4@ZIF-8 nanocomposite to activate sodium percarbonate for highly effective degradation of organic compound in aqueous solution, Journal of Industrial and Engineering Chemistry, 68 (2018) 406-415.

[55] M.P. Rayaroth, U.K. Aravind, C.T. Aravindakumar, Degradation of pharmaceuticals by ultrasound-based advanced oxidation process, Environmental Chemistry Letters, 14 (2016) 259-290.

[56] A.R. Khataee, M. Safarpour, M. Zarei, S. Aber, Electrochemical generation of H_2O_2 using immobilized carbon nanotubes on graphite electrode fed with air: Investigation of operational parameters, Journal of Electroanalytical Chemistry, 659 (2011) 63-68.

[57] K.H. Chu, Y.A.J. Al-Hamadani, C.M. Park, G. Lee, M. Jang, A. Jang, N. Her, A. Son, Y. Yoon, Ultrasonic treatment of endocrine disrupting compounds, pharmaceuticals, and personal care products in water: A review, Chemical Engineering Journal, 327 (2017) 629-647.

[58] J.-K. Im, J. Heo, L.K. Boateng, N. Her, J.R.V. Flora, J. Yoon, K.-D. Zoh, Y. Yoon, Ultrasonic degradation of acetaminophen and naproxen in the presence of single-walled carbon nanotubes, Journal of Hazardous Materials, 254-255 (2013) 284-292.

[59] R. Xiao, Z. He, D. Diaz-Rivera, G.Y. Pee, L.K. Weavers, Sonochemical degradation of ciprofloxacin and ibuprofen in the presence of matrix organic compounds, Ultrasonics Sonochemistry, 21 (2014) 428-435.

[60] R. Xiao, Z. Wei, D. Chen, L.K. Weavers, Kinetics and Mechanism of Sonochemical Degradation of Pharmaceuticals in Municipal Wastewater, Environmental Science & Technology, 48 (2014) 9675-9683.

[61] R.A. Al-Juboori, T. Yusaf, V. Aravinthan, L. Bowtell, Investigating natural organic carbon removal and structural alteration induced by pulsed ultrasound, Science of The Total Environment, 541 (2016) 1019-1030.

[62] L. Yang, J.F. Rathman, L.K. Weavers, Degradation of Alkylbenzene Sulfonate Surfactants by Pulsed Ultrasound, The Journal of Physical Chemistry B, 109 (2005) 16203-16209.

[63] R. Darvishi Cheshmeh Soltani, M. Safari, Periodate-assisted pulsed sonocatalysis of real textile wastewater in the presence of MgO nanoparticles: Response surface methodological optimization, Ultrasonics Sonochemistry, 32 (2016) 181-190.

[64] M.D.G. de Luna, M.L. Veciana, C.-C. Su, M.-C. Lu, Acetaminophen degradation by electro-Fenton and photoelectro-Fenton using a double cathode electrochemical cell, Journal of Hazardous Materials, 217-218 (2012) 200-207.

[65] N. Villota, J.M. Lomas, L.M. Camarero, Study of the paracetamol degradation pathway that generates color and turbidity in oxidized wastewaters by photo-Fenton technology, Journal of Photochemistry and Photobiology A: Chemistry, 329 (2016) 113-119.

Figures captions

Fig. 1. FE-SEM images of magnetite nanostructures taken at different scales (a) and (b), together with corresponding XRD pattern (c).

Fig. 2. FE-SEM image of CB (a-1), XRD pattern of CB (a-2), FE-SEM image of CC (b-1), XRD pattern of CC (b-2), FE-SEM image of CB-coated CC (c-1), and XRD pattern of CB-coated CC (c-2).

Fig. 3. TGA/DTG curves obtained for uncoated CC (a) and CB-coated CC (b).

Fig. 4. Contribution of each process involved in the integrated process in removing APAP. Experimental conditions: $[APAP]_0$: 5 mg/L, current: 0.1 A, initial pH: natural (5.5), electrolyte concentration: 0.04 M, US frequency: 37 kHz, US power: 100%.

Fig. 5. Influence of initial pH in the range of 3-9 (a), current in the range of 0.05-0.15 A (b), APAP concentration in the range of 3-10 mg/L (c), and electrolyte concentration in the range of 0.02-0.07 M (d) on the degradation efficiency of APAP by the integrated process. Experimental conditions: Reaction time: 90 min, US frequency: 37 kHz, US power: 100%.

Fig. 6. Effects of US irradiation mode, US power, and US frequency on the removal efficiency of APAP. Experimental conditions: $[APAP]_0$: 5 mg/L, current: 0.1 A, initial pH: natural (5.5), electrolyte concentration: 0.04 M.

Fig. 7. Schematic flow-diagram of intermediates produced during the decomposition of APAP by US/NADC-ECP.

Fig. 8. Variations of I_{OUR} (%) for each treatment process involved in removing APAP versus reaction time.

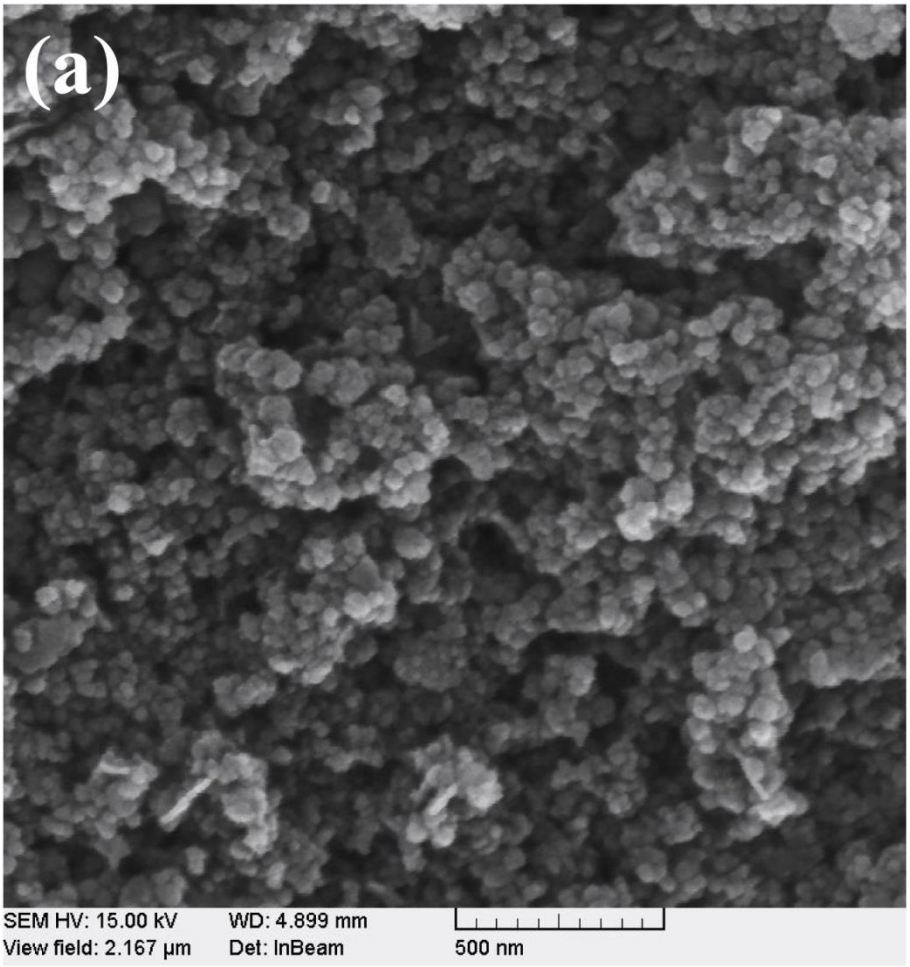

Fig. 1 (a)

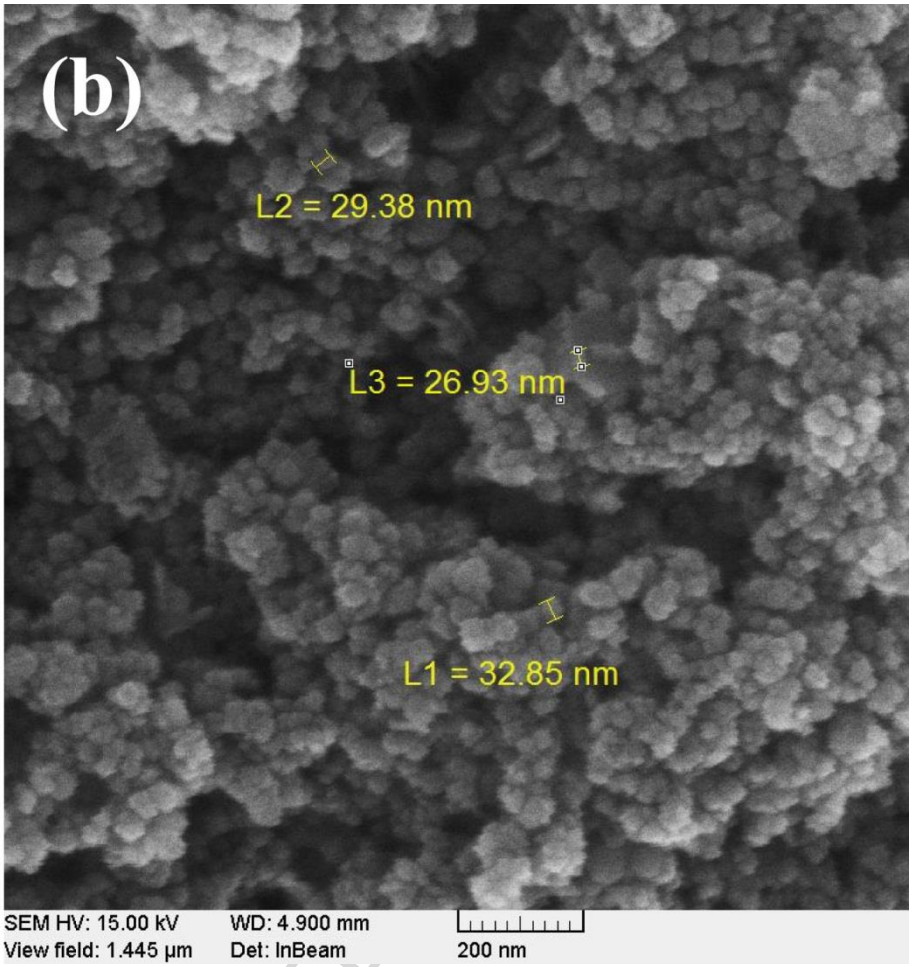

Fig. 1 (b)

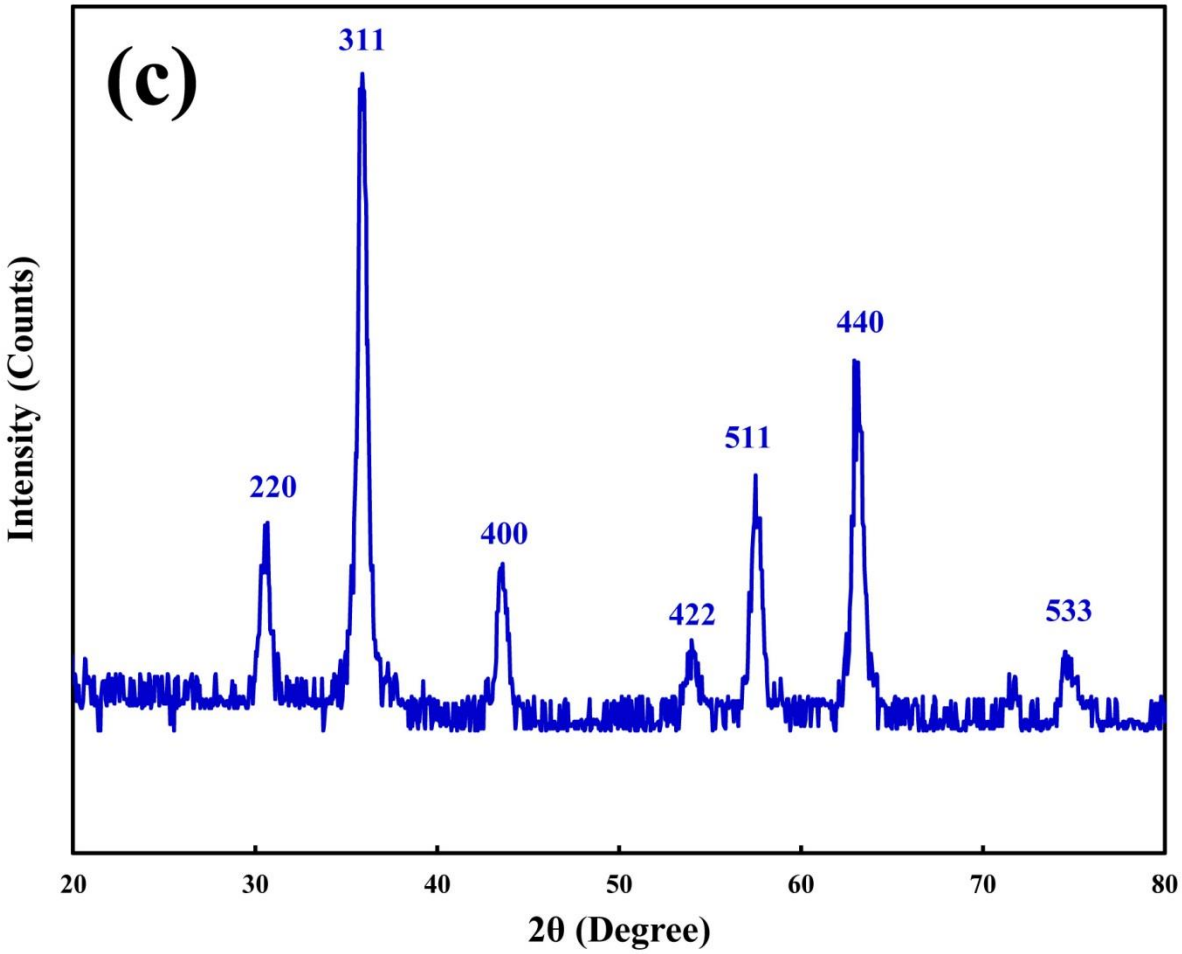

Fig. 1 (c)

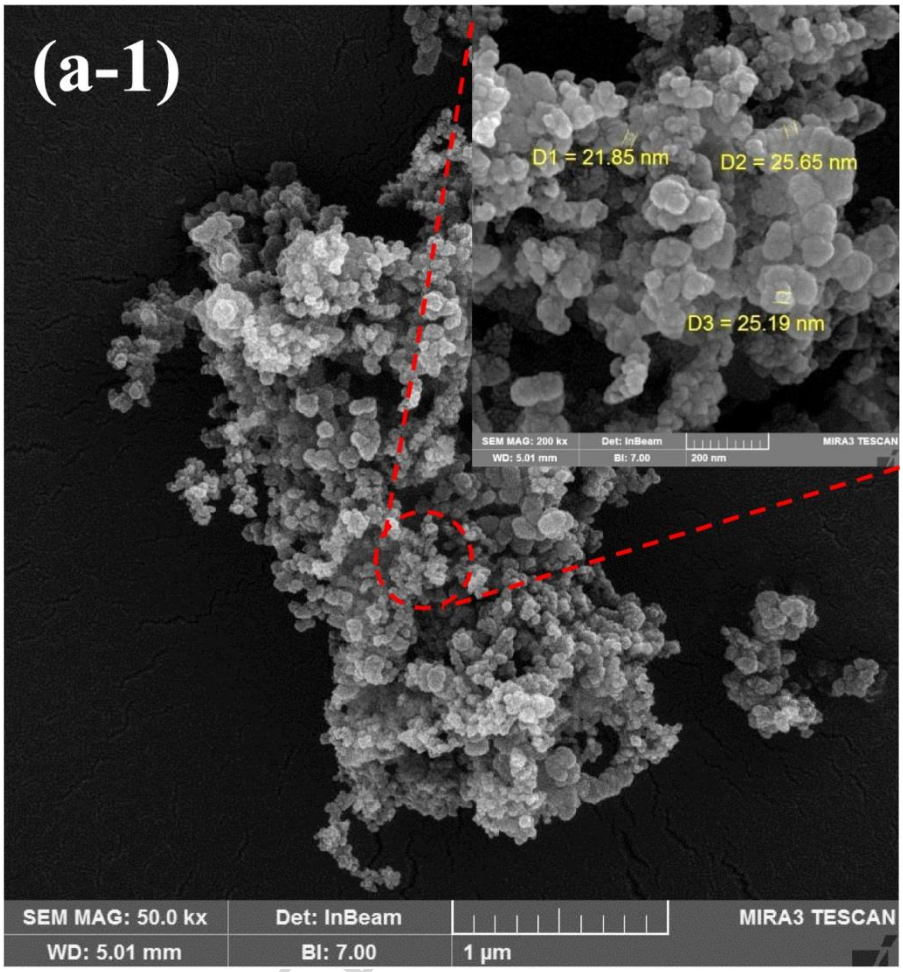

Fig. 2 (a-1)

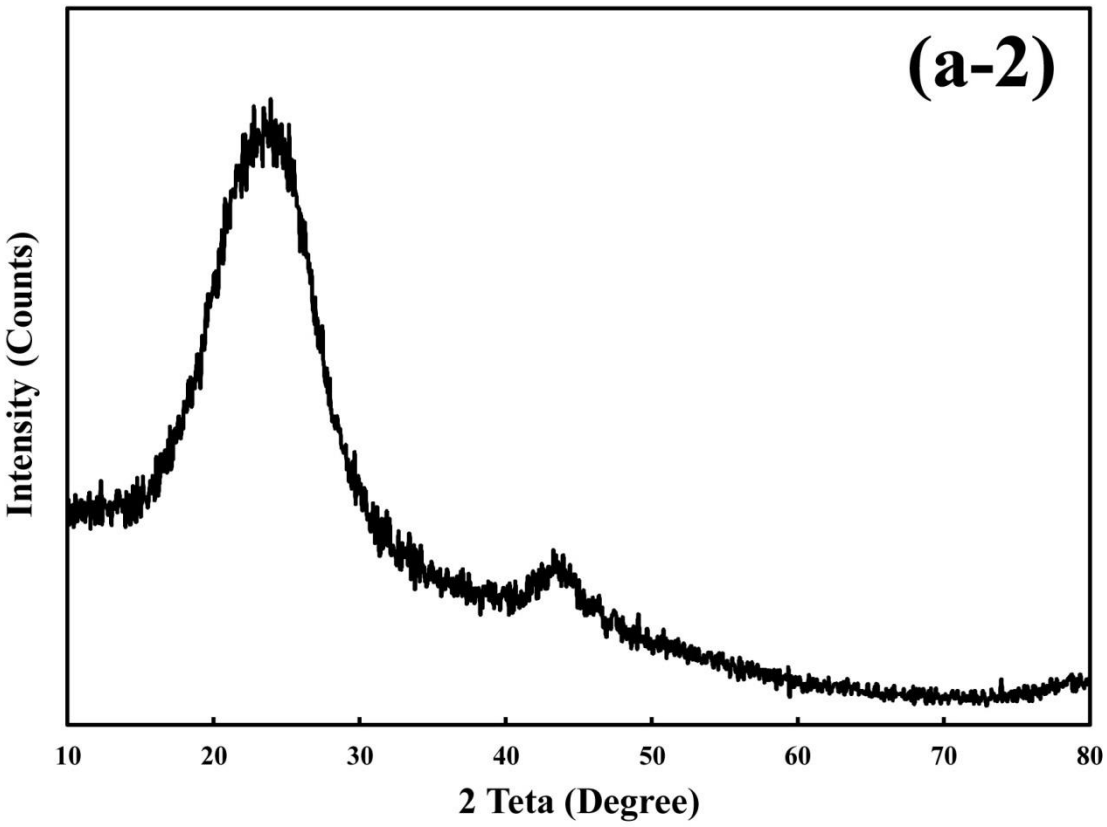

Fig. 2 (a-2)

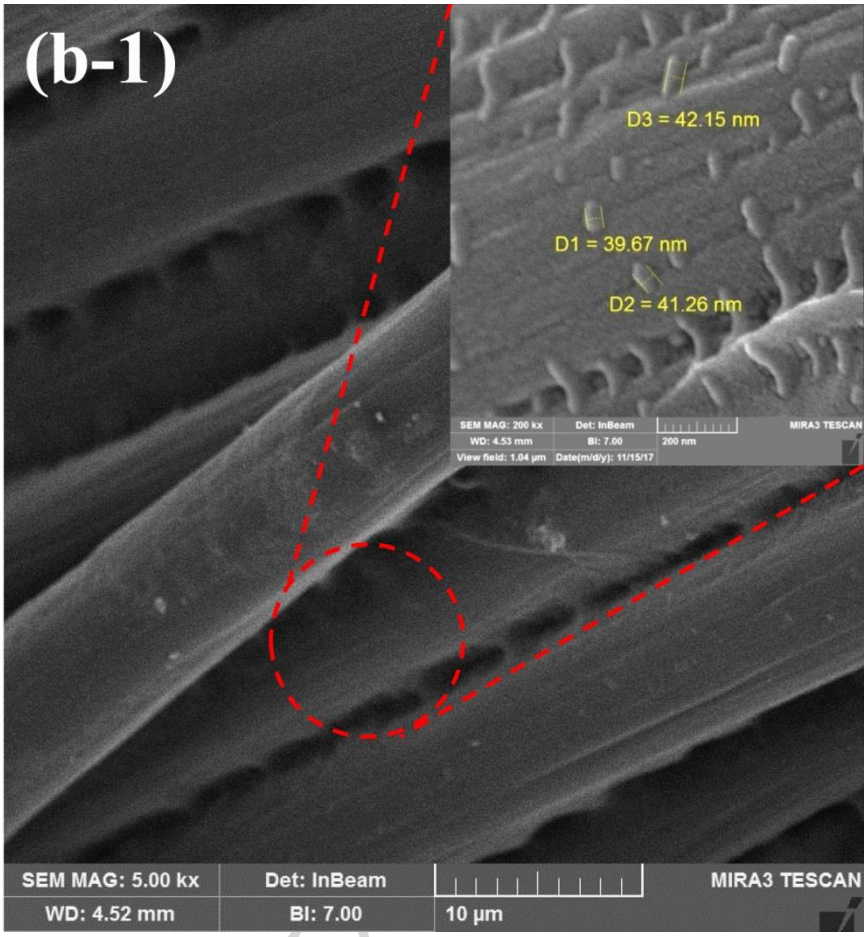

Fig. 2 (b-1)

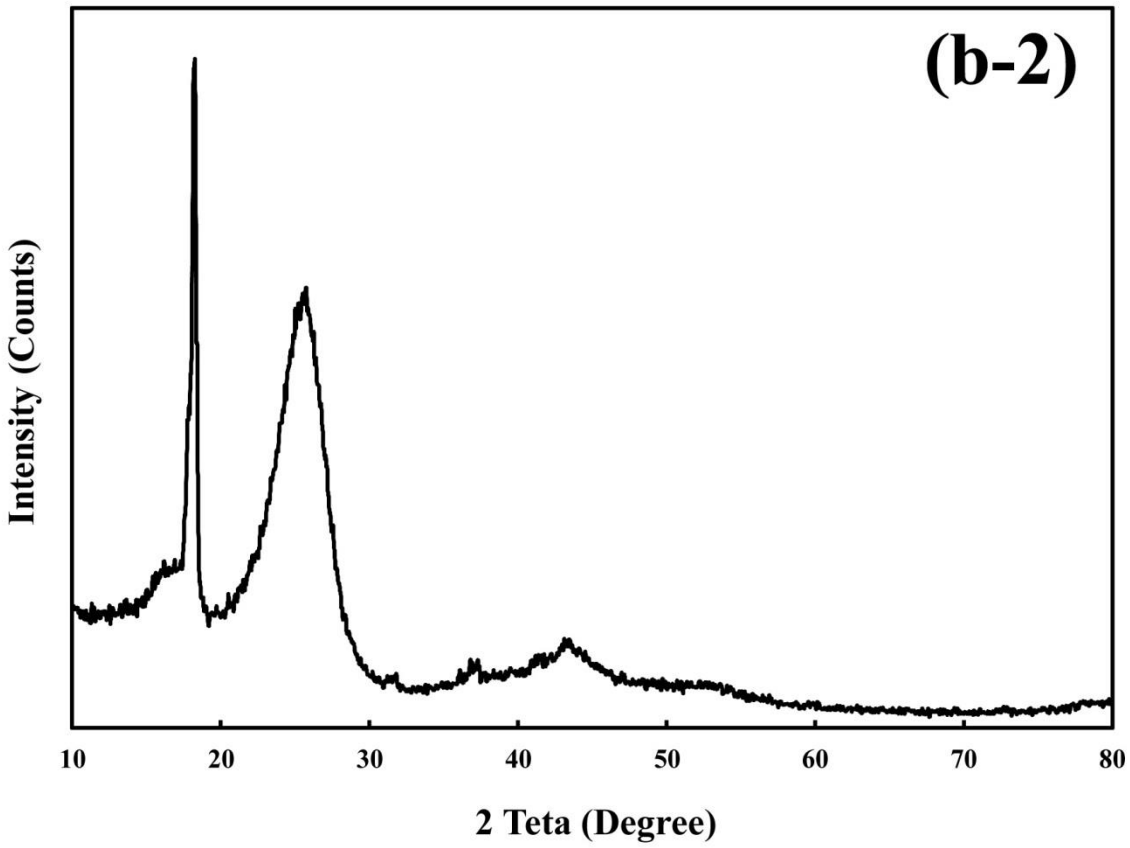

Fig. 2 (b-2)

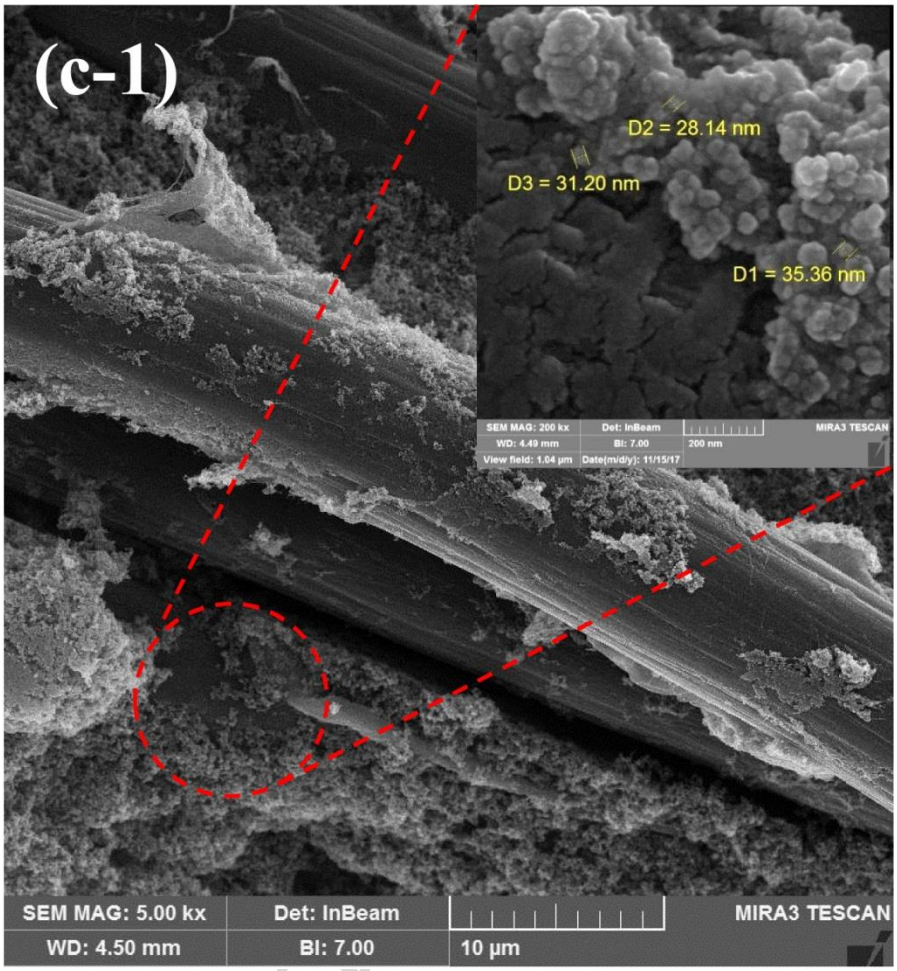

Fig. 2 (c-1)

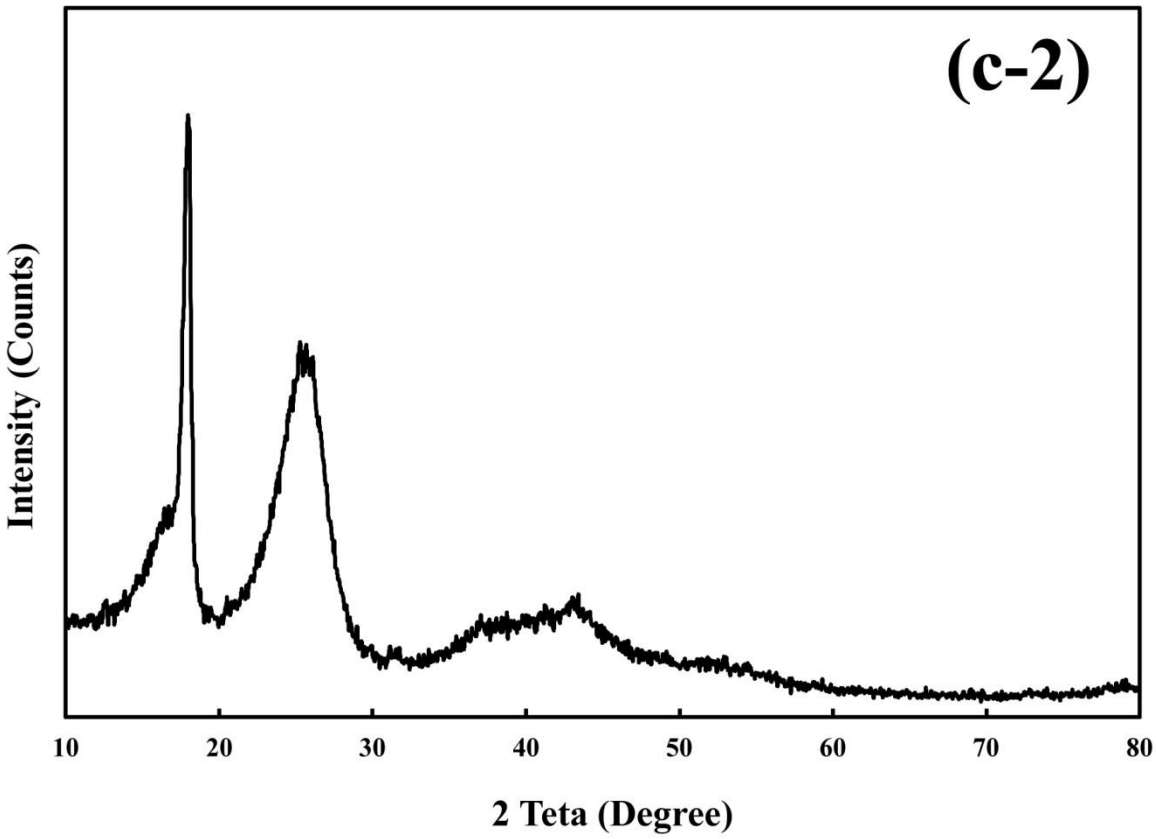

Fig. 2 (c-2)

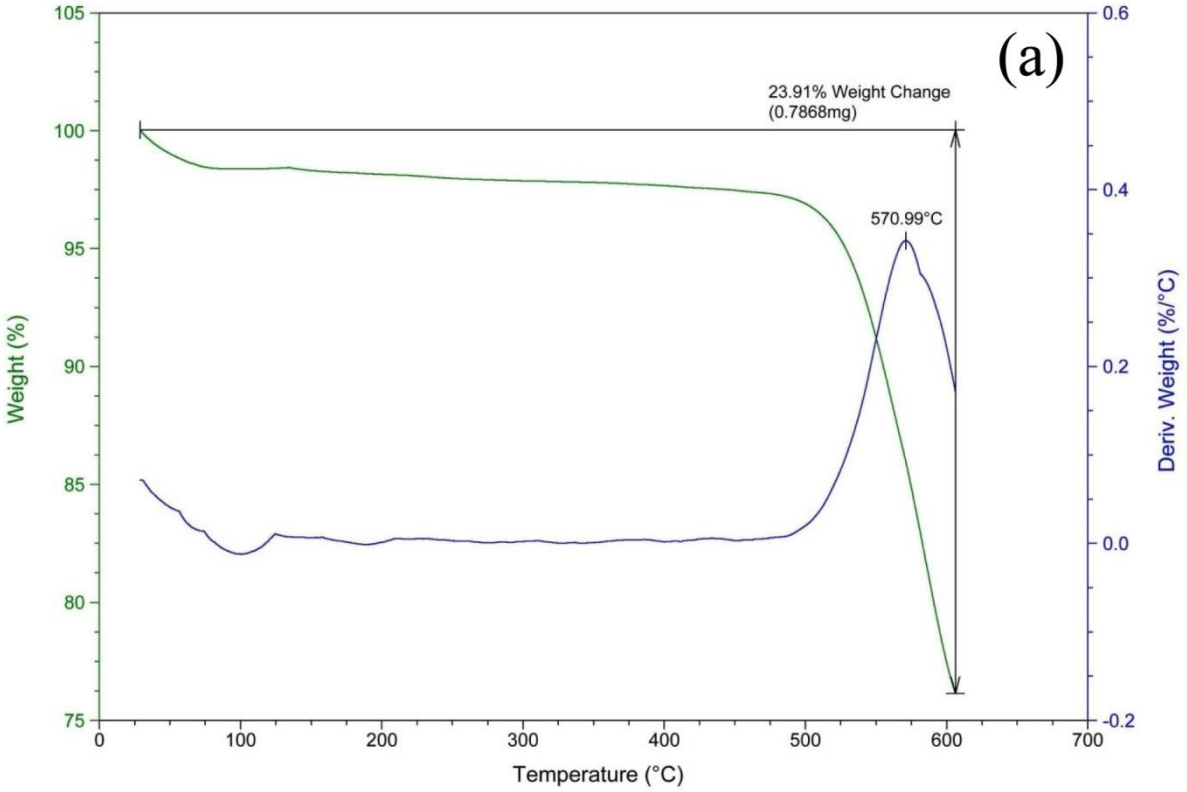

Fig. 3 (a)

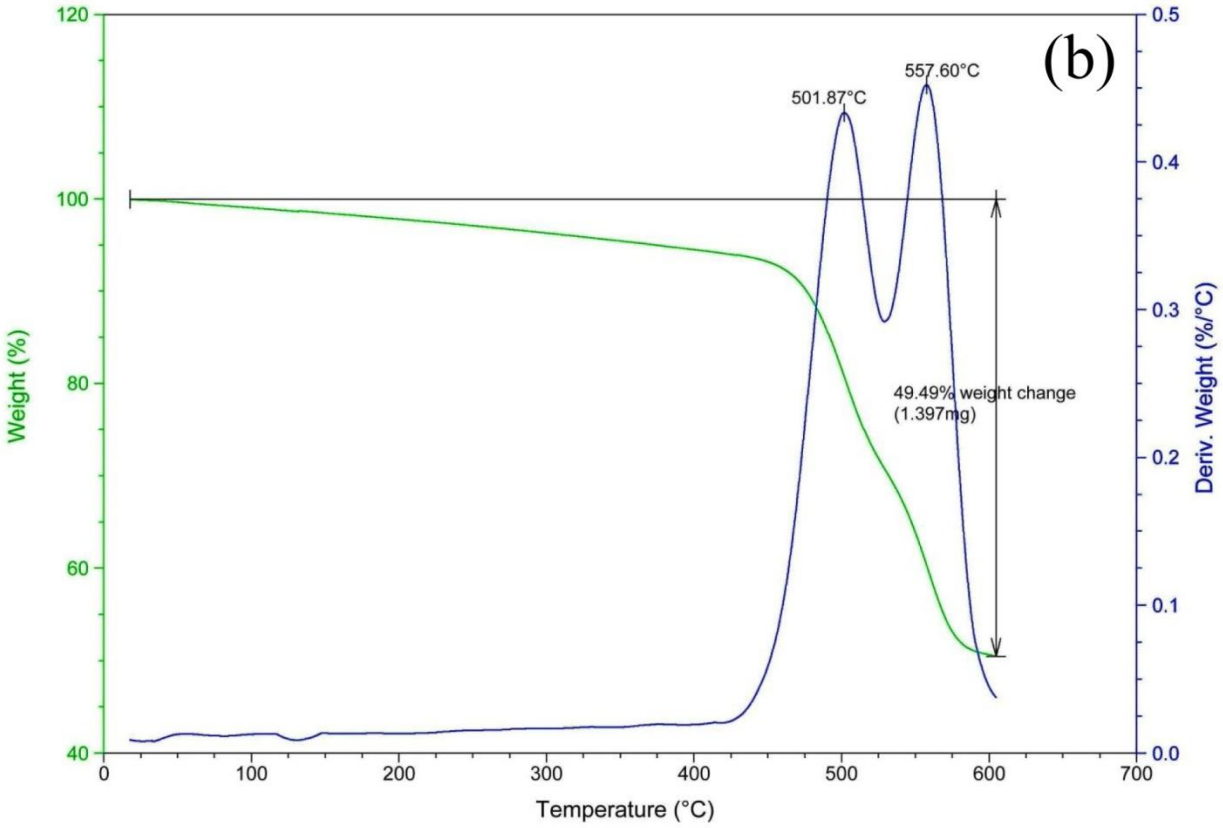

Fig. 3 (b)

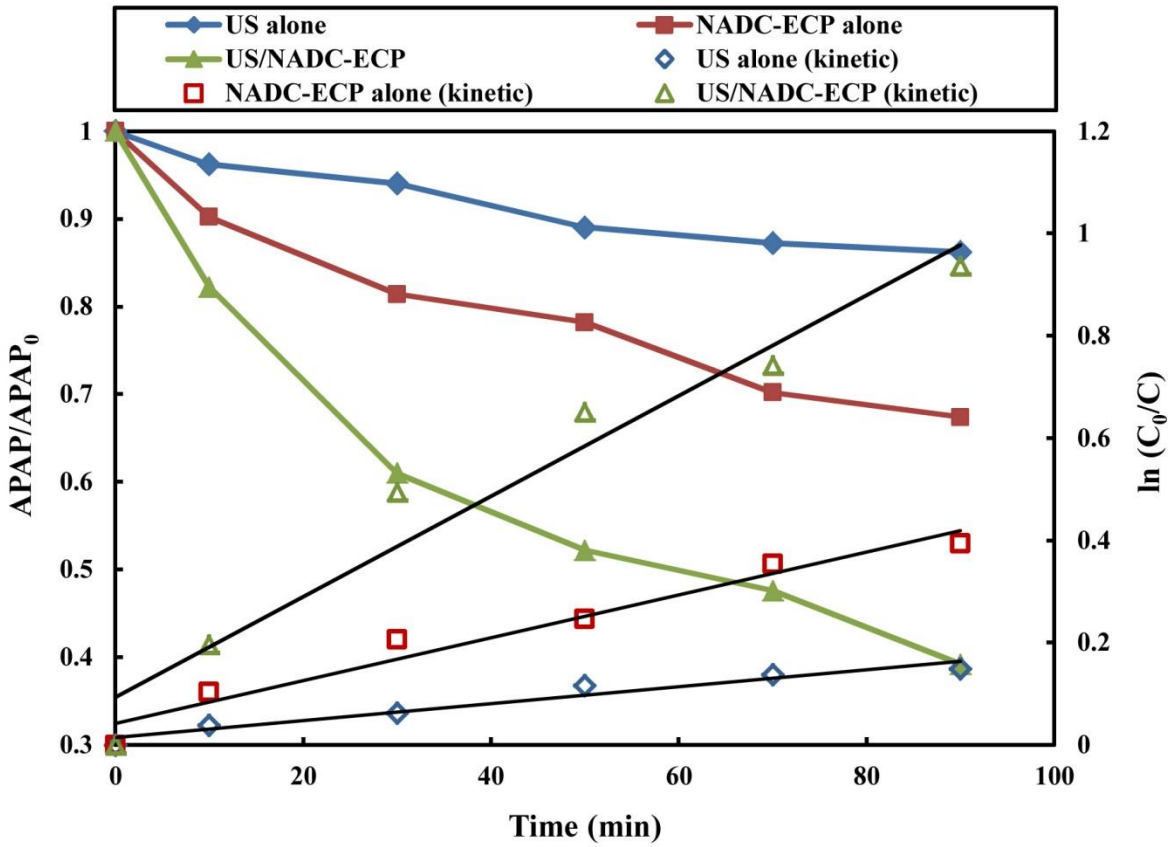

Fig. 4

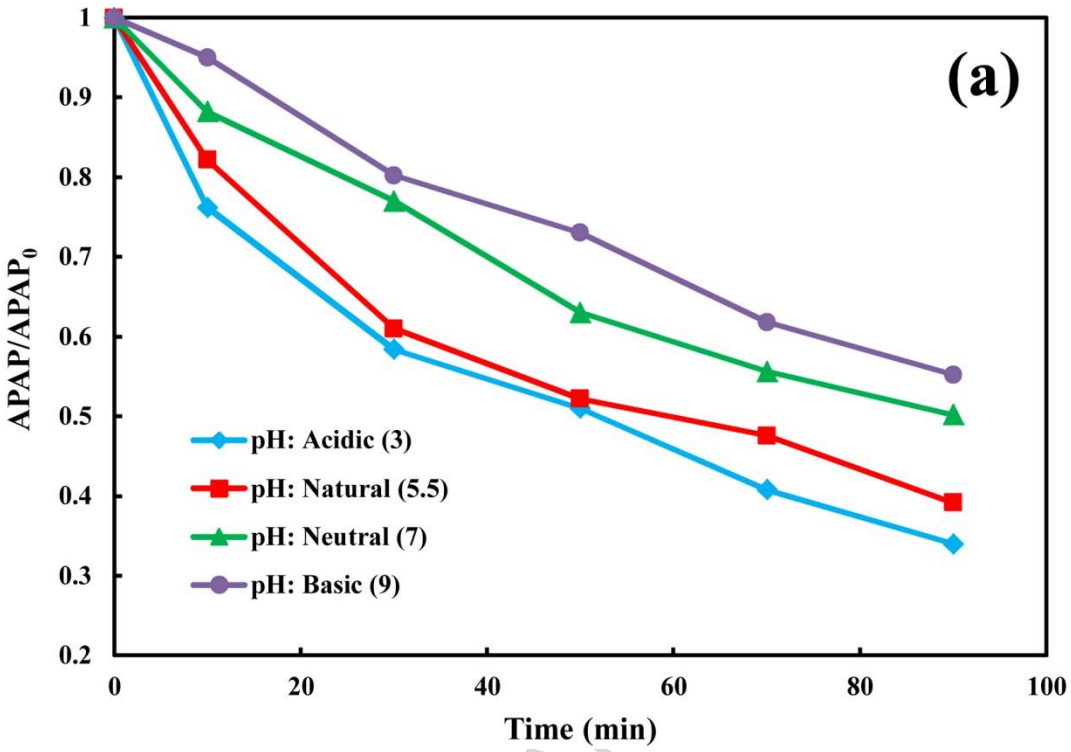

Fig. 5 (a)

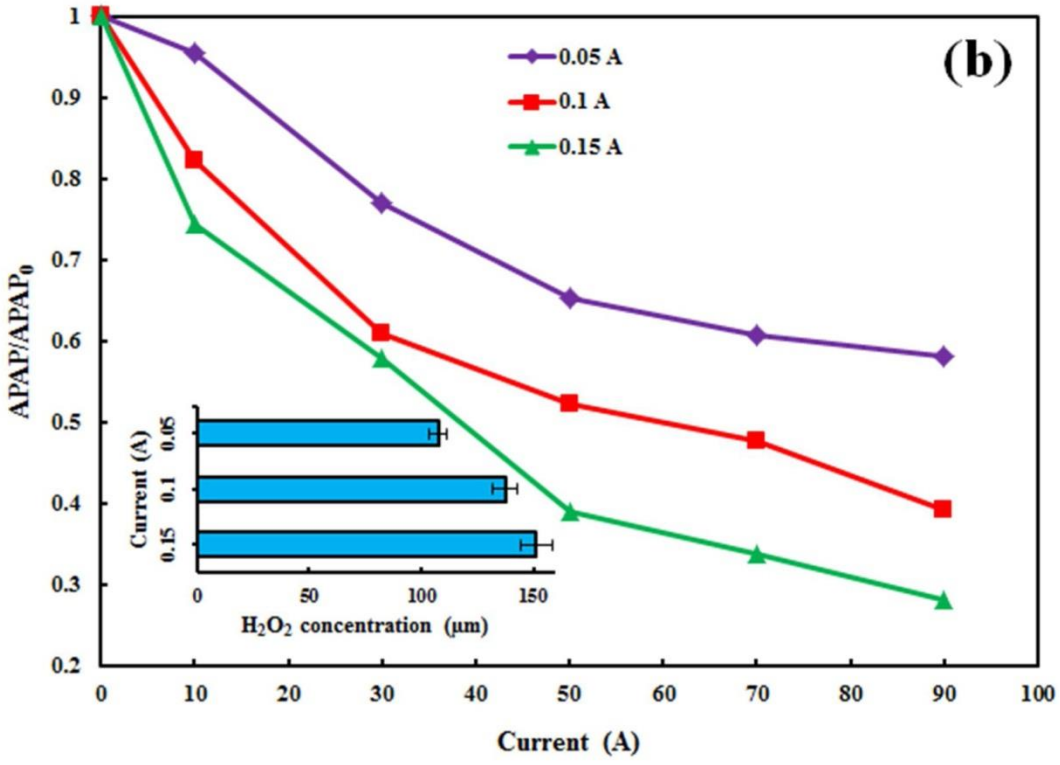

Fig. 5 (b)

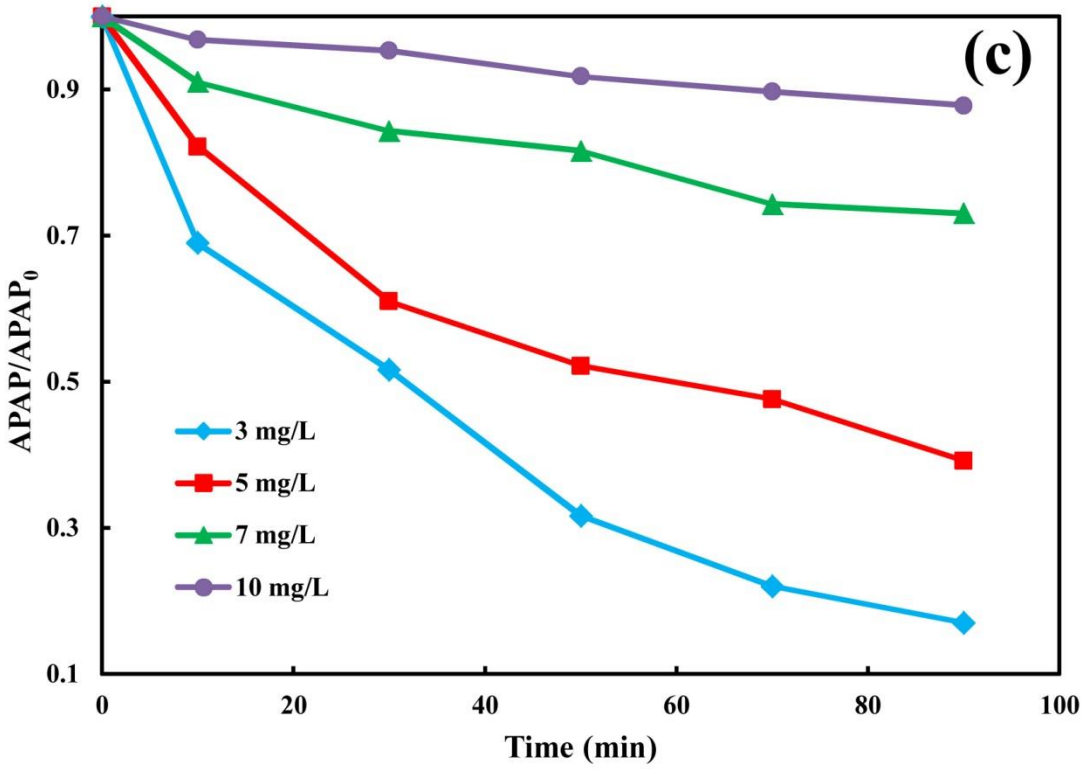

Fig. 5 (c)

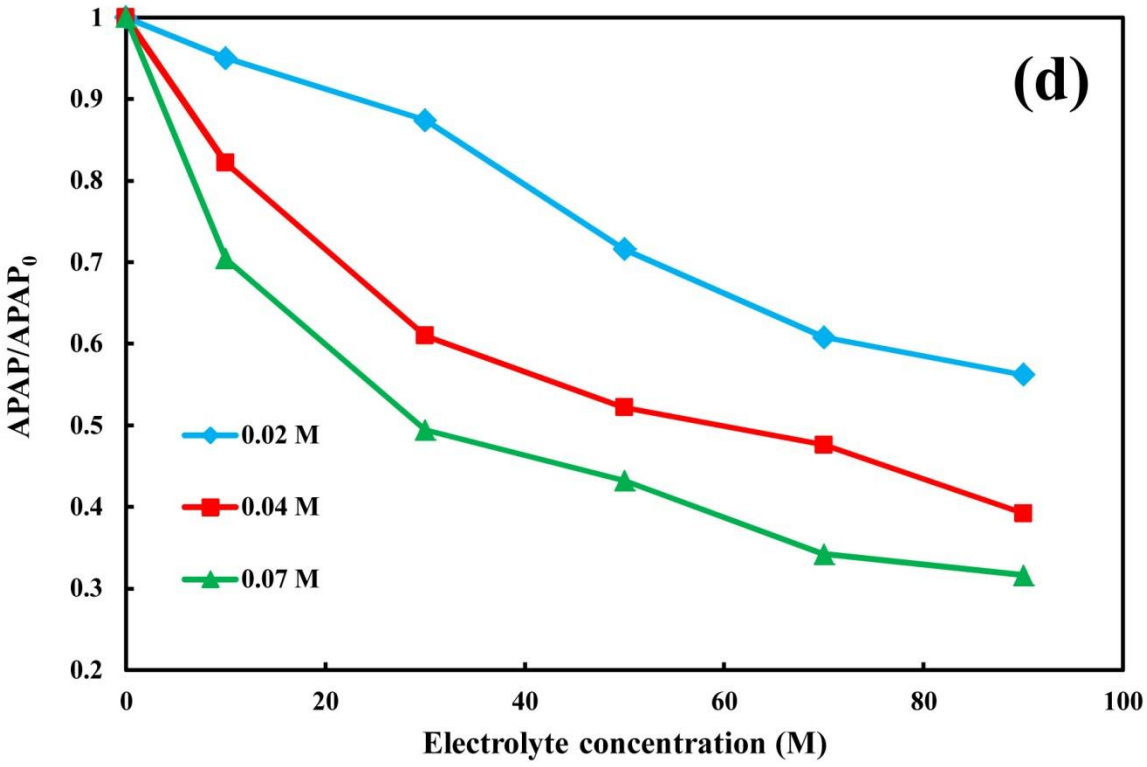

Fig. 5 (d)

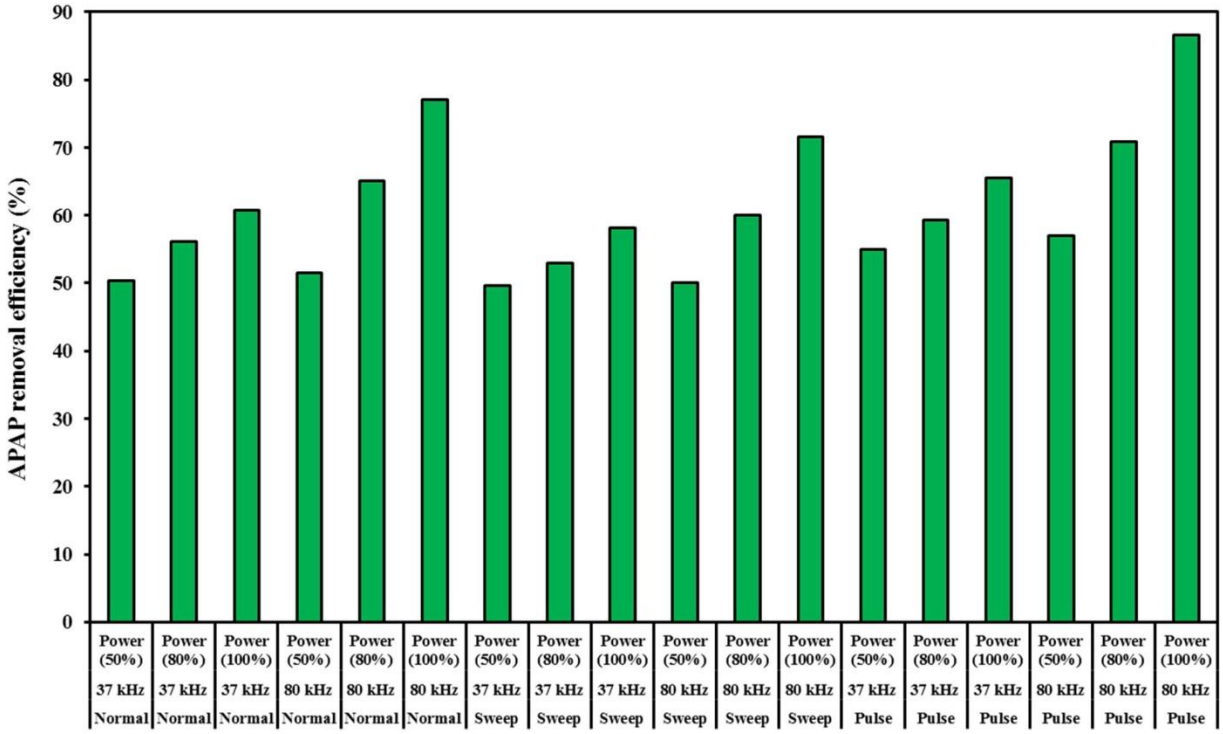

Fig. 6

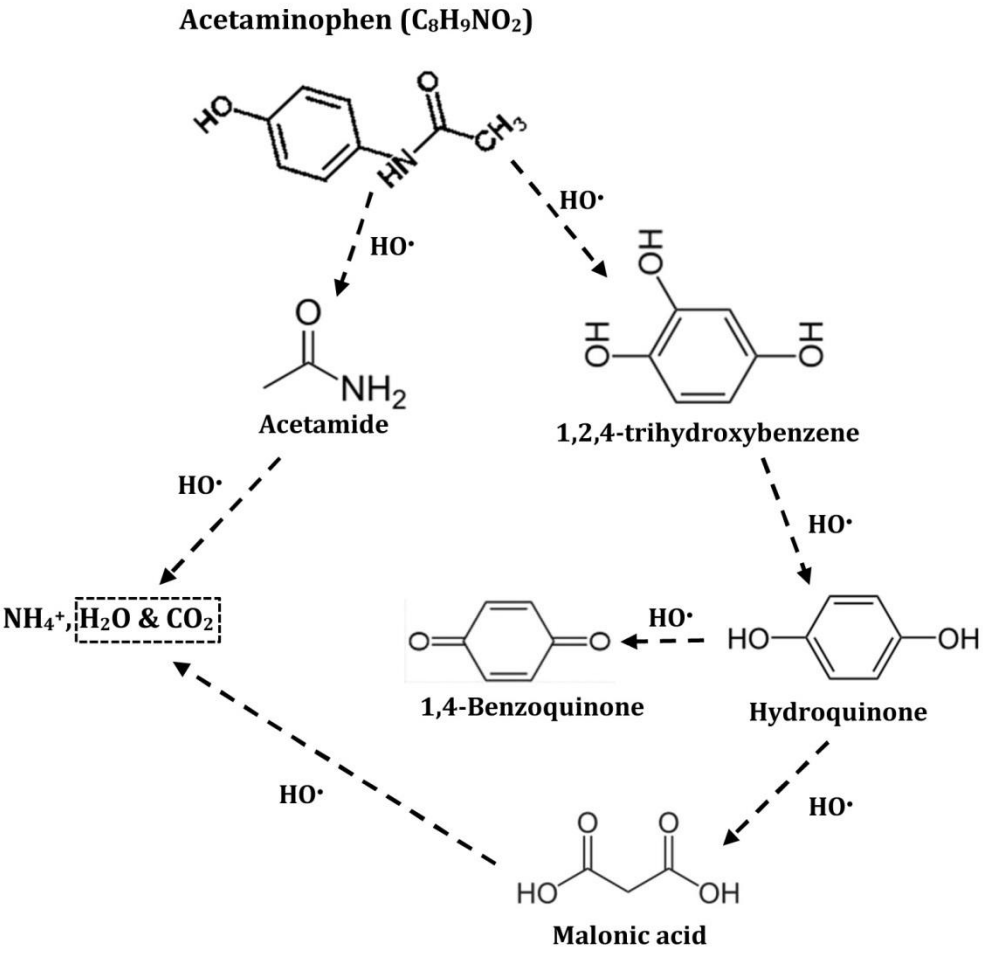

Fig. 7

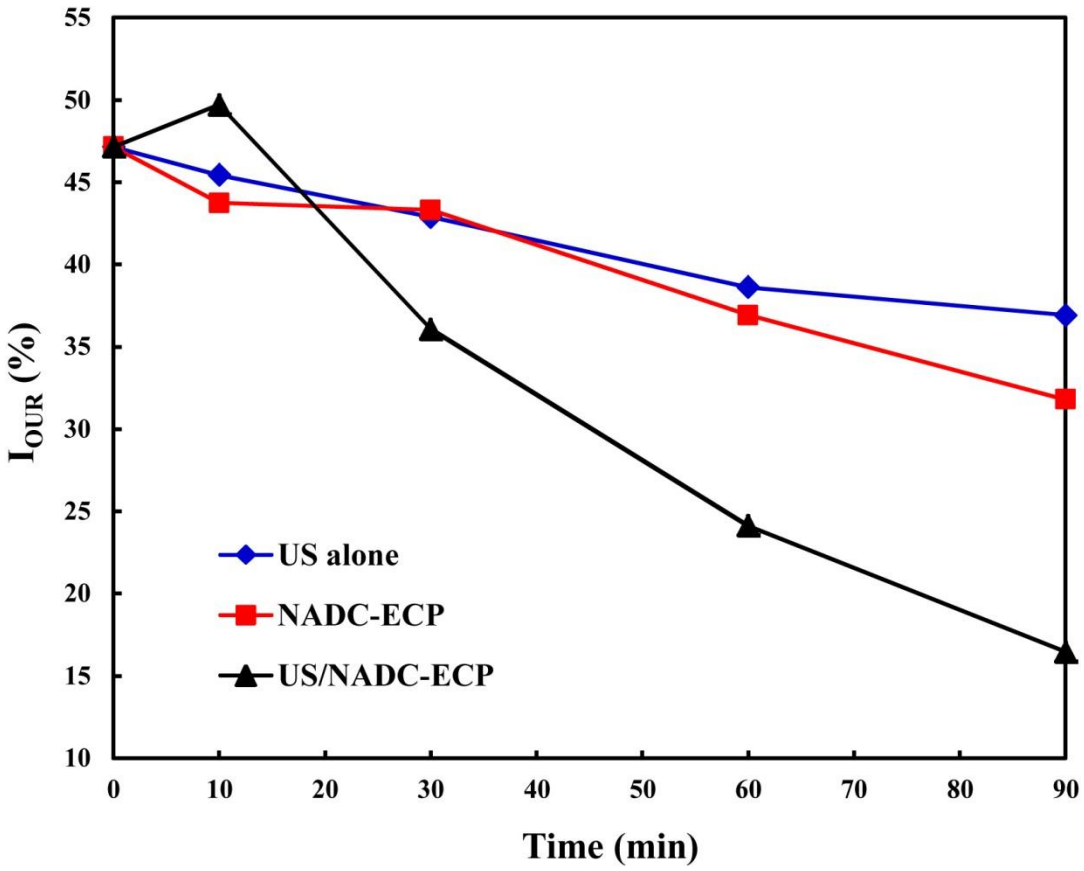

Fig. 8

Table 1. Results of isotherm modeling for the adsorption of APAP onto $Fe^{2+}Fe^{3+}{}_2O_4$ nanostructures.

Types of isotherm models					
Langmuir model			**Freundlich model**		
q_m (mg/g)	K (L/mg)	R^2	K_F (mg/g)	n	R^2
2.76	0.29	0.99	1.19	4.75	0.95

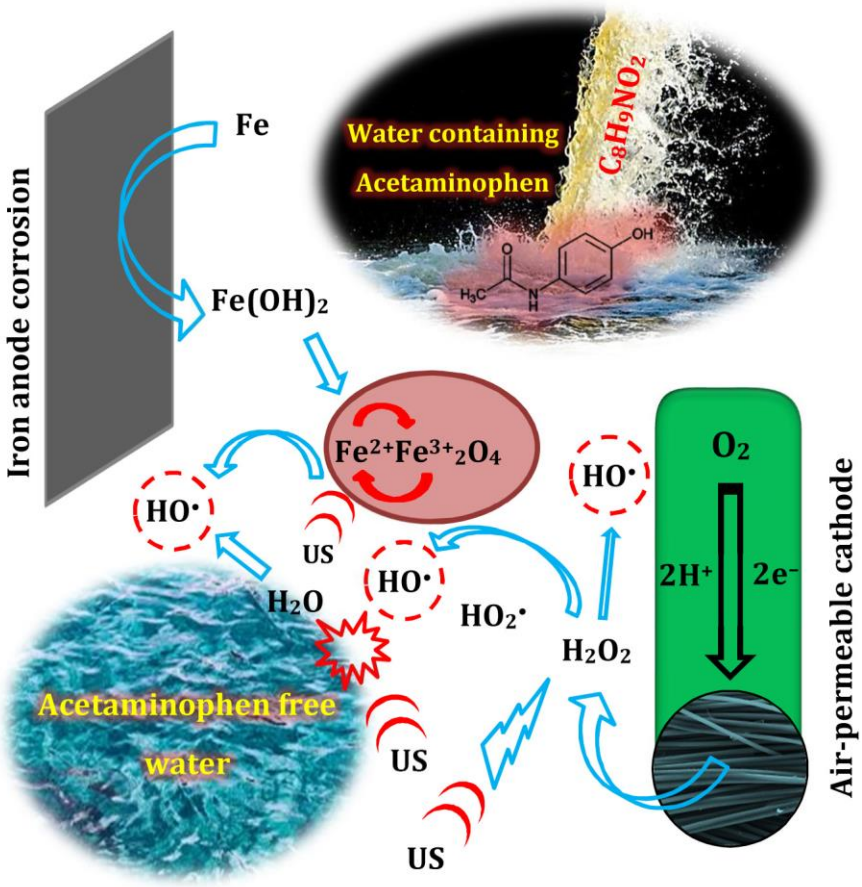

Graphical abstract

Research highlights

- ✓ Coupling carbon cloth (CC)-carbon black (CB) cathode with as-generated $Fe^{2+}Fe^{3+}{}_2O_4$.
- ✓ Verification of electro-generation of nanostructured $Fe^{2+}Fe^{3+}{}_2O_4$ via iron sacrifice anode.
- ✓ Synergistic degradation of APAP owing to coupling ultrasound with CC-CB/$Fe^{2+}Fe^{3+}{}_2O_4$.
- ✓ Insignificant toxicity of effluent based on activated sludge inhibition test.

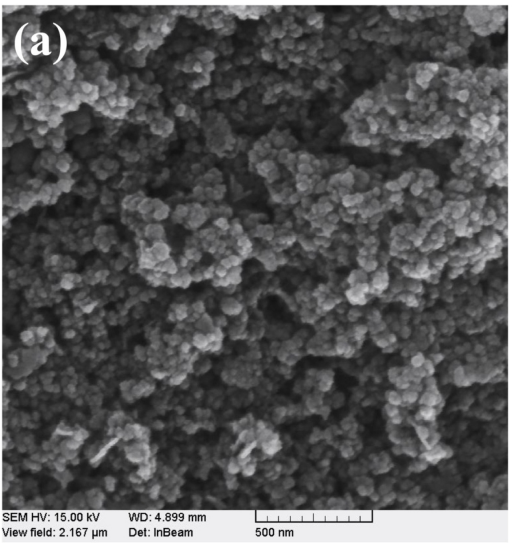

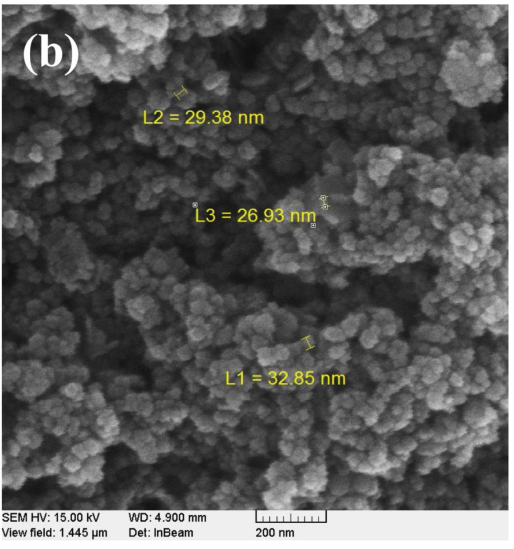

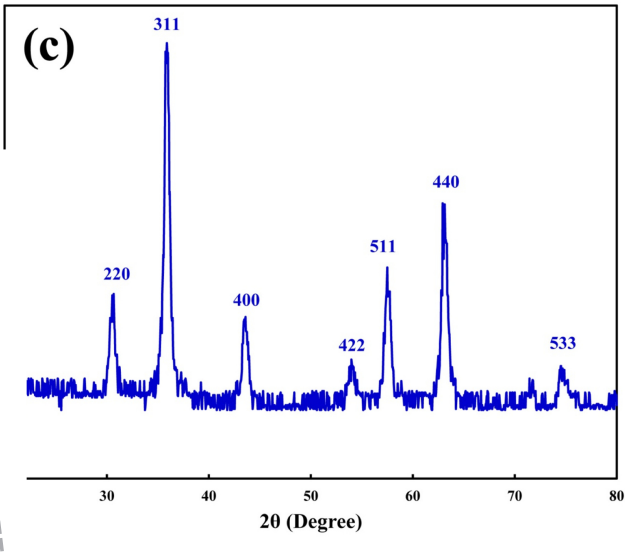

Figure 1

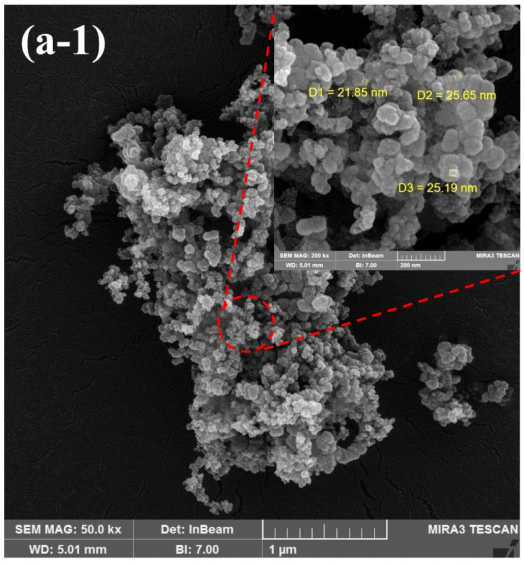

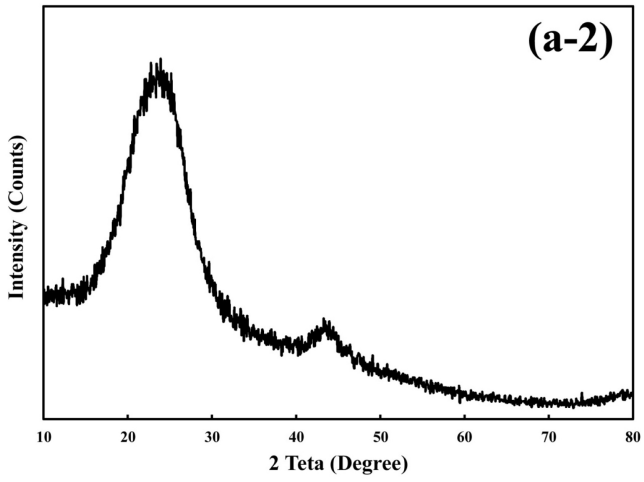

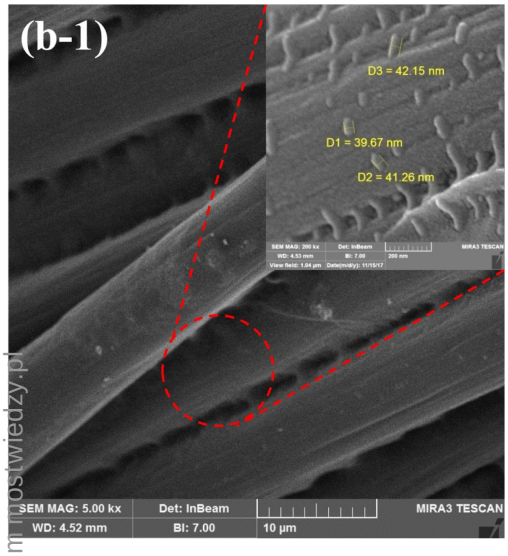

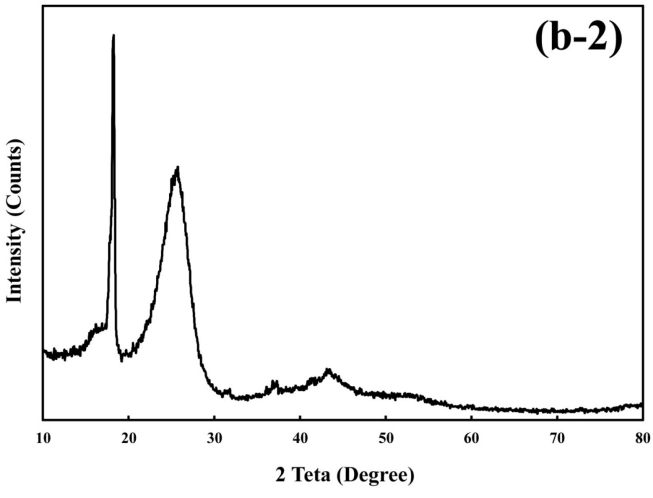

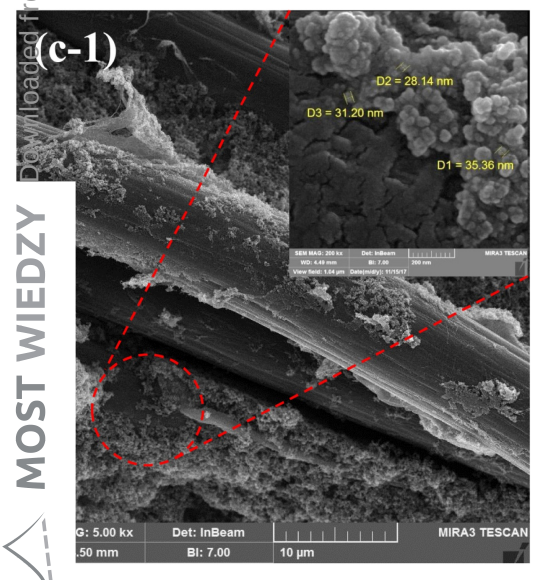

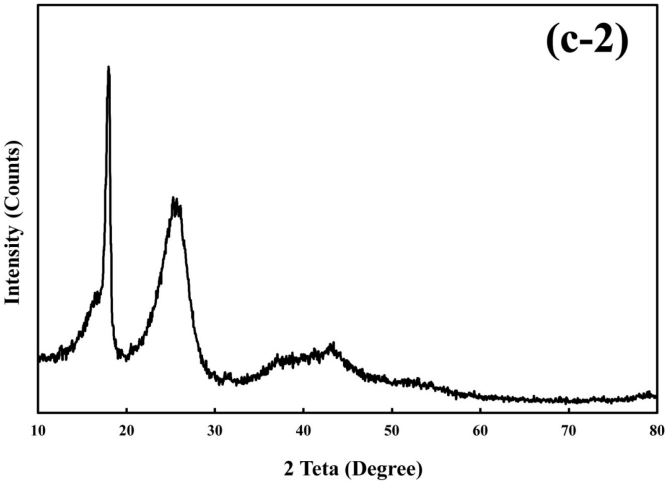

Figure 2

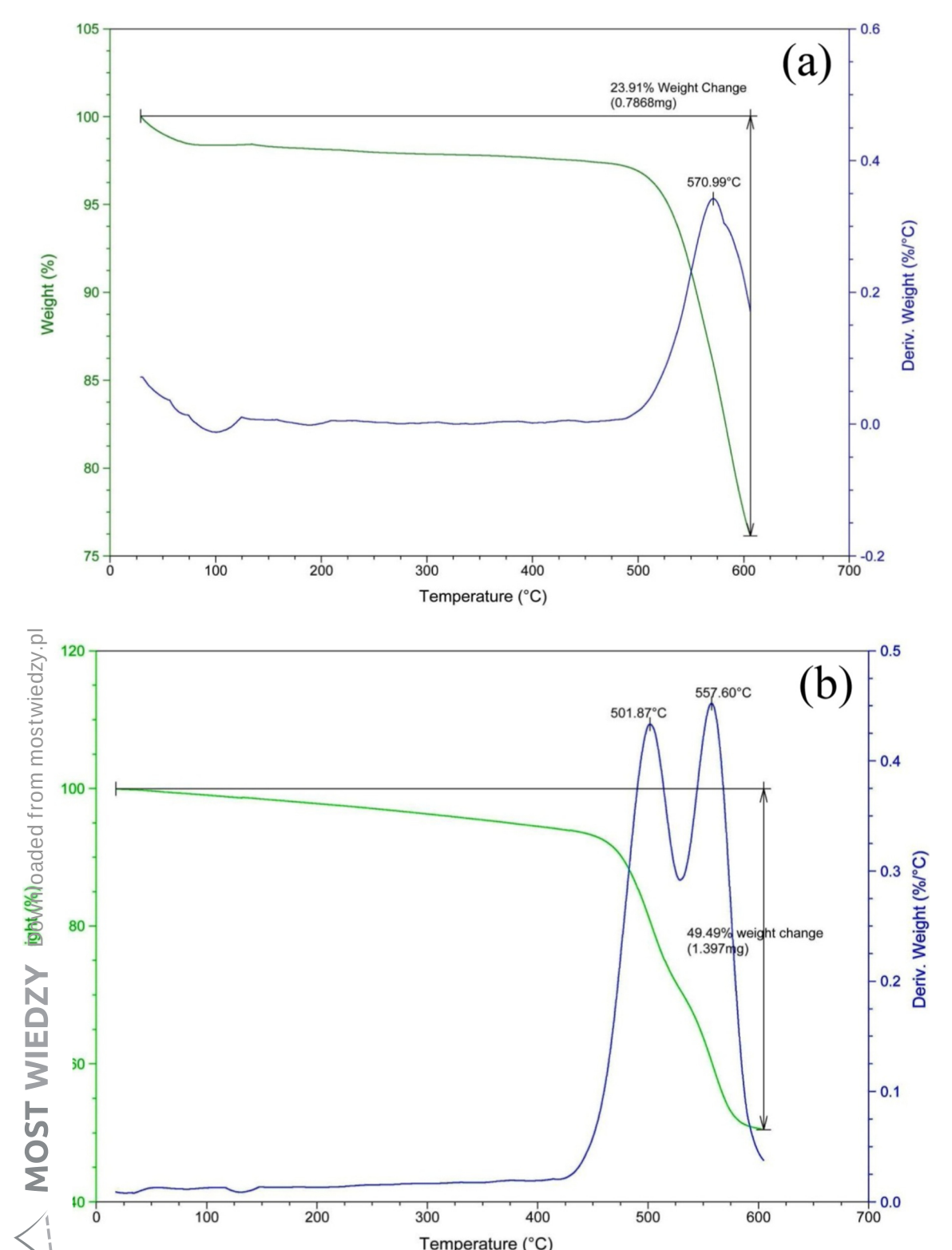

Figure 3

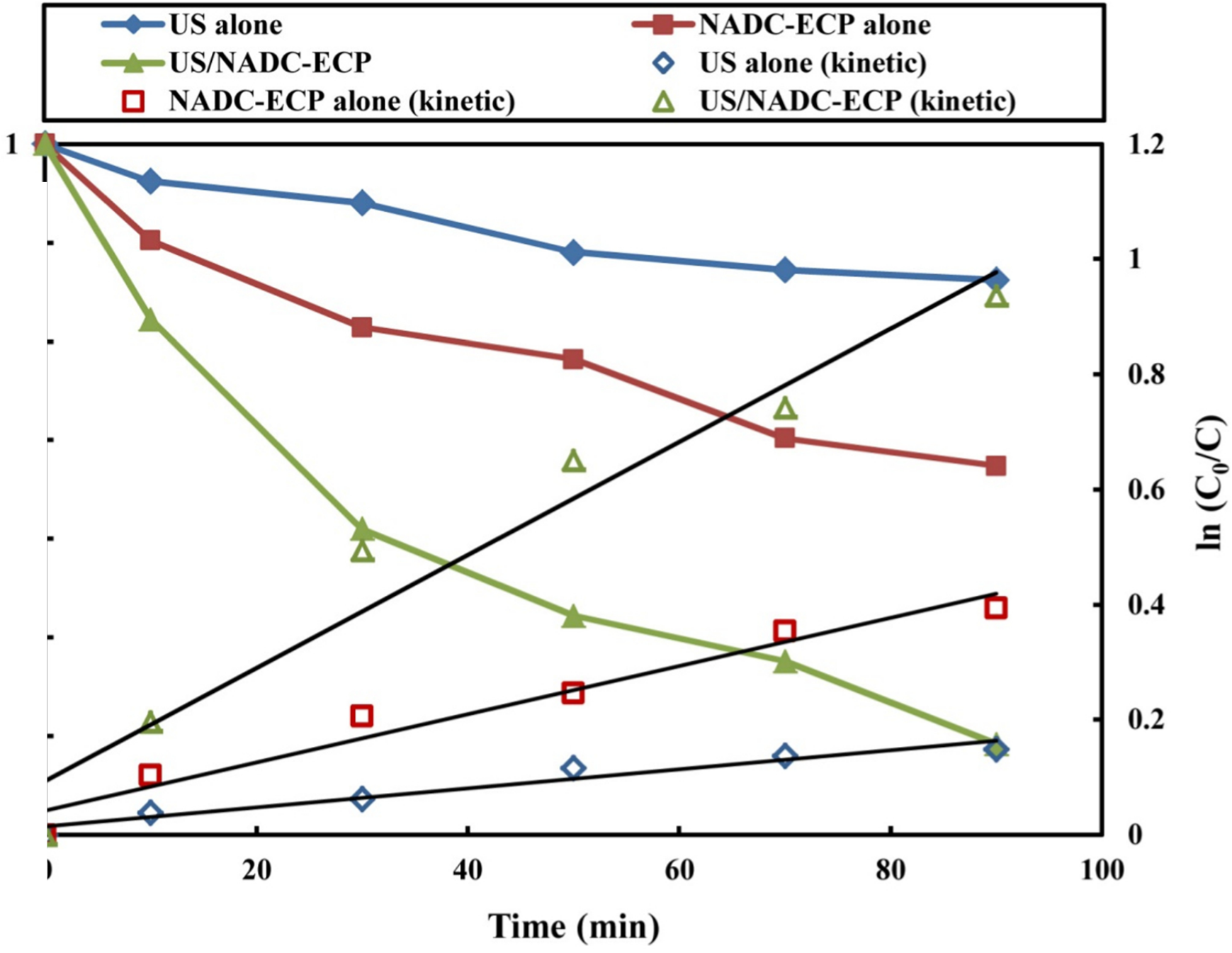

Figure 4

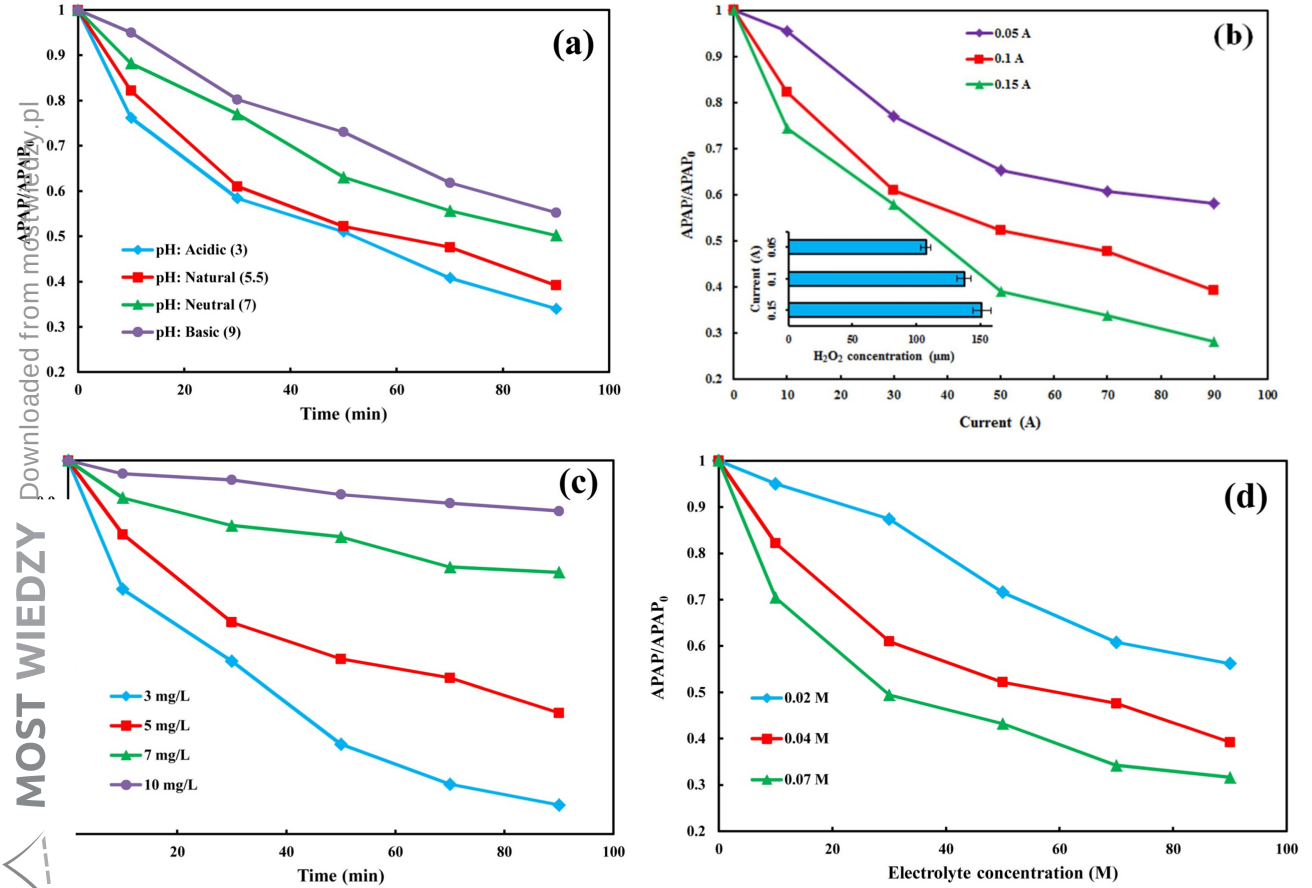

Figure 5

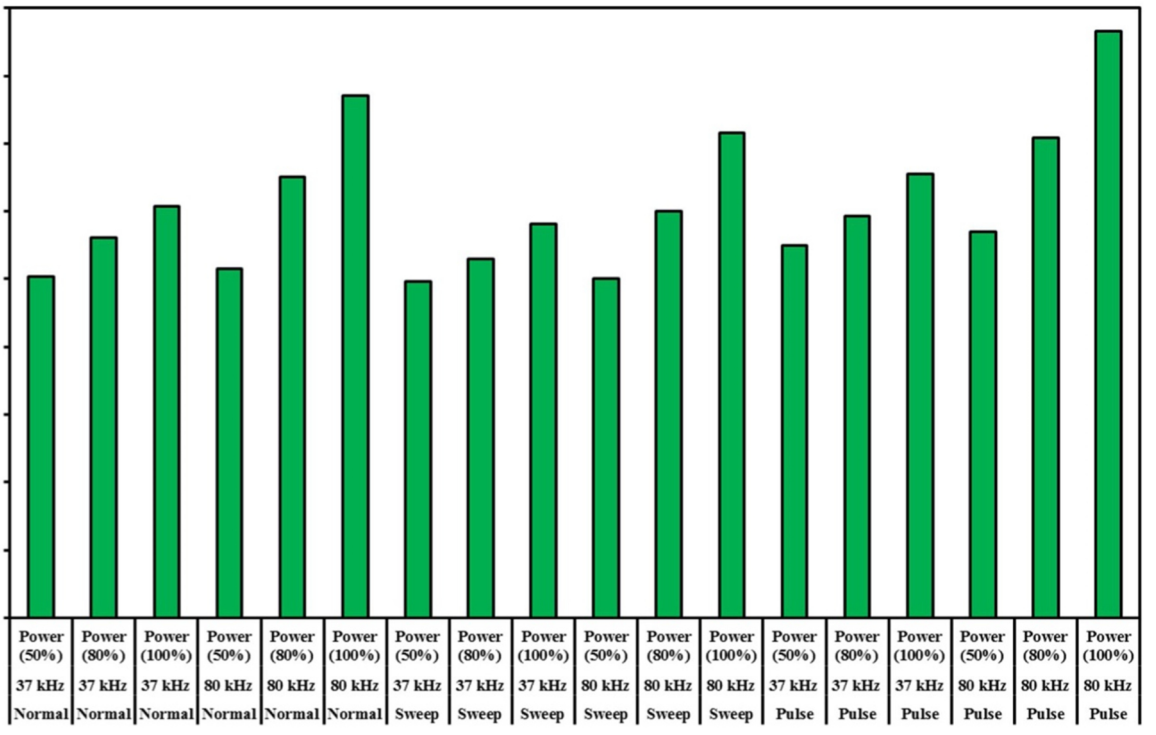

Figure 6

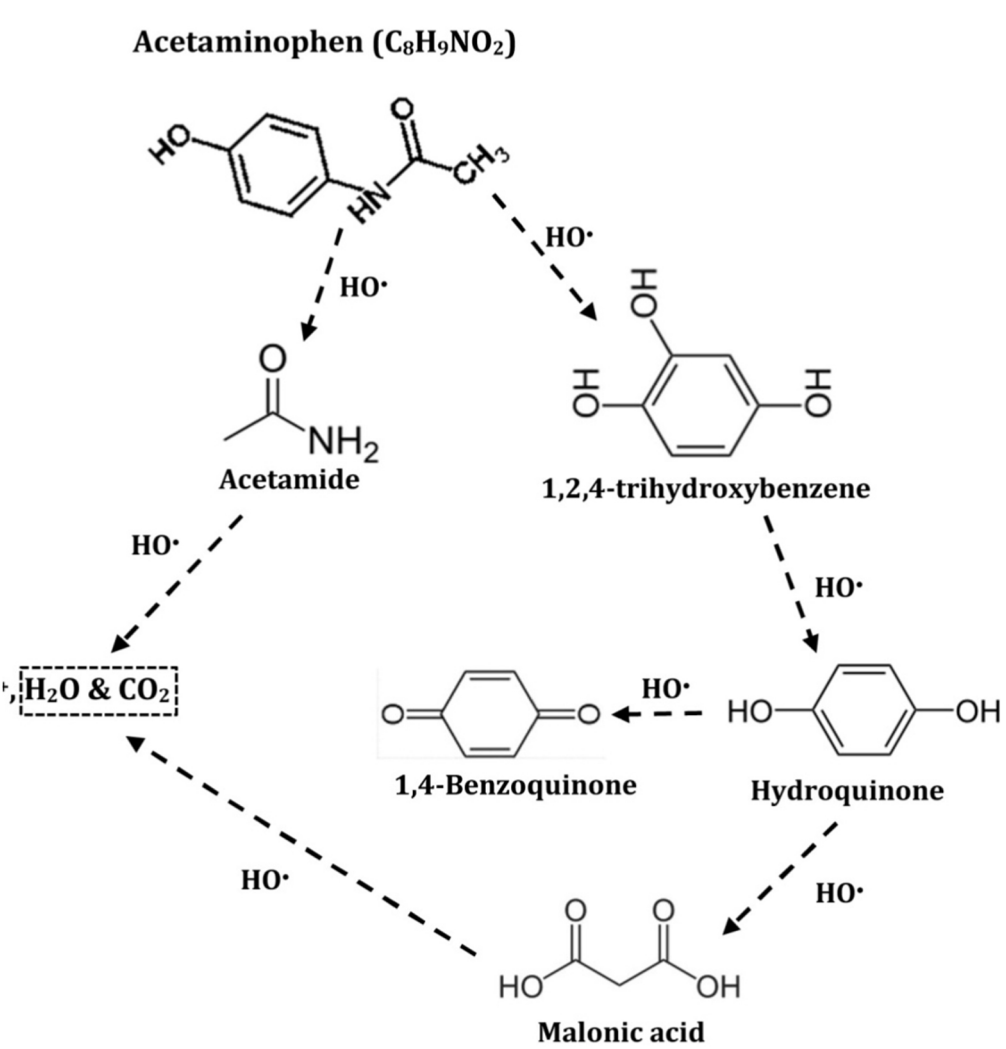

Figure 7

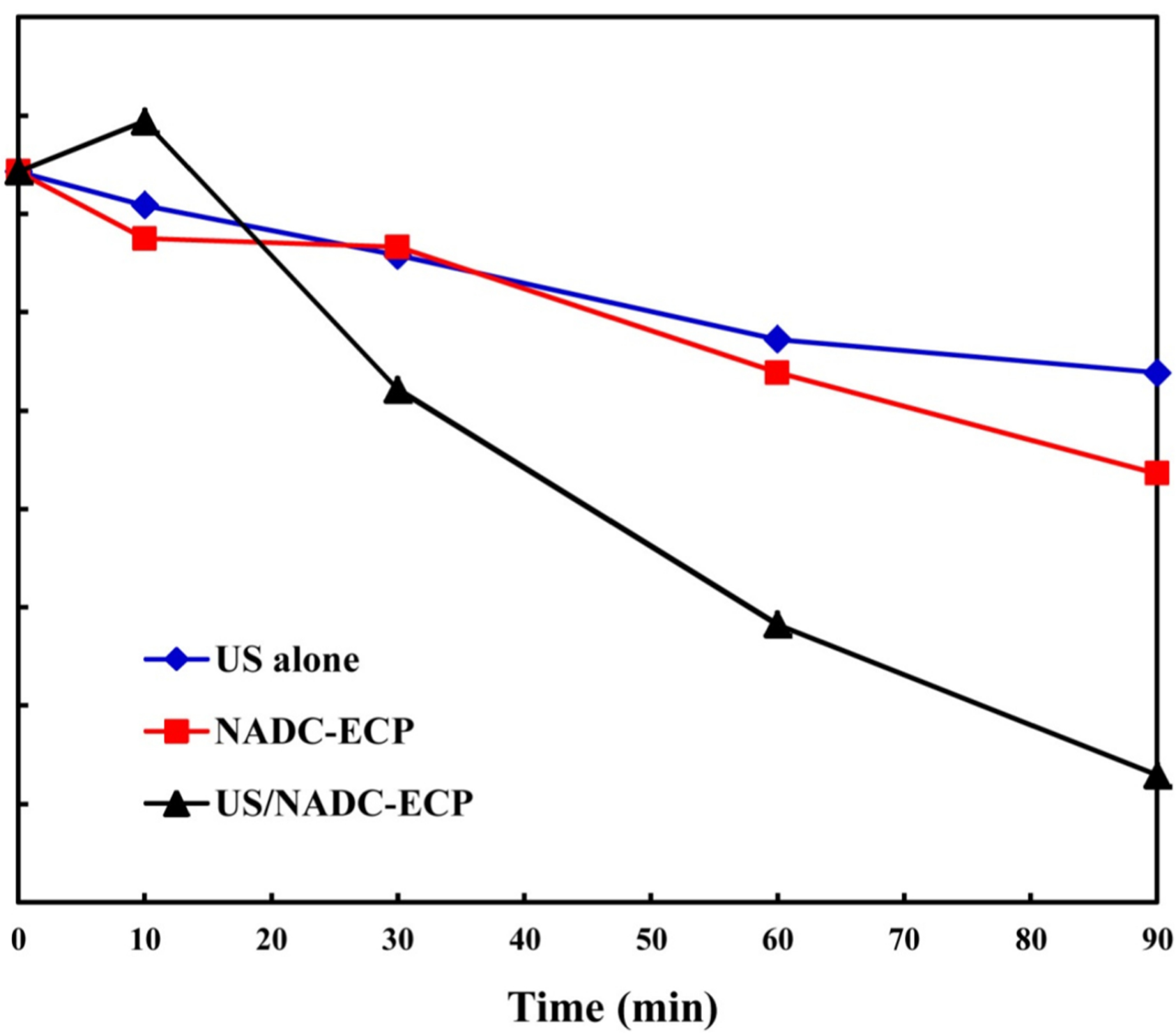

Figure 8